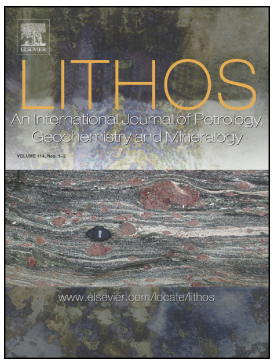

Implications of 770 Ma Rhyolitic Tuffs, eastern South China Craton in constraining the tectonic setting of the Nanhua Basin

Liang Qi, Yajun Xu, Peter A. Cawood, Wei Wang, Yuansheng Du

PII: S0024-4937(18)30466-3
DOI: https://doi.org/10.1016/j.lithos.2018.12.004
Reference: LITHOS 4895

To appear in: *LITHOS*

Received date: 27 September 2018
Accepted date: 5 December 2018

Please cite this article as: Liang Qi, Yajun Xu, Peter A. Cawood, Wei Wang, Yuansheng Du , Implications of 770 Ma Rhyolitic Tuffs, eastern South China Craton in constraining the tectonic setting of the Nanhua Basin. Lithos (2018), https://doi.org/10.1016/j.lithos.2018.12.004

Implications of 770 Ma Rhyolitic Tuffs, eastern South China Craton in constraining the tectonic setting of the Nanhua Basin

Liang Qi[1], Yajun Xu[1,*] xuyajun19@163.com , Peter A. Cawood[2,3], Wei Wang[1], Yuansheng Du[1]

[1]State Key Laboratory of Geological Processes and Mineral Resources, Center for Global Tectonics, School of Earth Sciences, China University of Geosciences, Wuhan, 430074, China

[2]School of Earth, Atmosphere & Environment, Monash University, Melbourne, VIC 3800, Australia

[3]Department of Earth Sciences, University of St. Andrews, North Street, St. Andrews KY16 9AL, UK

[*]Corresponding author.

Abstract

Mid-Neoproterozoic magmatic rocks from the southeastern part of the Nanhua Basin constrain the tectonic setting of the basin. Data from rhyolitic tuffs of the Louqian Formation that overlie the Cathaysia Block in southeastern South China indicate accumulation of the unit at ca. 770 Ma, and provide an upper age limit on collisional assembly of the Yangtze and Cathaysia blocks. The zircons within the tuffs display largely positive $\varepsilon_{Hf}(t)$ (-3.66 to +13.94) and juvenile T_{DM} (Hf) values (1.74-0.90 Ga), which indicate involvement of Neoproterozoic to late Paleoproterozoic crustal materials in their generation. Geochemically, the tuffs are peraluminous and characterized by both A-type and arc affinities with high SiO_2, Ga, accentuated negative Eu anomalies, strong depletion in high field strength elements and high zircon saturation temperatures (T_{Zr}), which are comparable to contemporaneous (800-750 Ma) felsic rocks from the northwestern of the Nanhua Basin. These characteristics suggest the Nanhua Basin lay inboard of a convergent plate margin arc. This arc is represented by 860-730 Ma magmatism along the western and northern margin of the South China Craton (Panxi-Hannan Belt), with the Nanhua Basin occupying an upper plate, back arc setting.

Keywords: Nanhua Basin, Mid-Neoproterozoic, Louqian Formation, Rhyolite tuff, Back-arc setting.

1. Introduction

Mid-Neoproterozoic magmatic rocks (830-730 Ma) are widespread on several continental fragments including South China, India, Madagascar, Australia, Laurentia

and Seychelles (Archibald et al., 2017; Ashwal et al., 2013; Li et al., 2008a; Wang et al., 2010; Zhou et al., 2007). This period coincides with the break-up of Rodinia (Powell et al.,1993;Li et al., 2008b)and the formation of the Nanhua Basin in South China. The Nanhua Basin succeeded the amalgamation of the Yangtze and Cathaysia blocks to form the unified South China Craton (Zheng et al., 2008; Zhao and Cawood, 2012). Previous geochronological and geochemical investigations within the basin have focused on the less deformed units overlying the Yangtze Block and Jiangnan Orogen, and indicate two phases of magmatism in the basin, with age peaks at ca. 820 Ma and ca. 770 Ma(Chen et al., 2018b; Zheng et al., 2008). Four possible models have proposed: (1) plume-rift model (Li et al., 2003; Li et al., 1999; Zhang et al., 2013).(2) plate-rift model (Wang et al., 2010; Zheng et al., 2008; Zheng et al., 2007), (3) slab-arc model (Zhou et al., 2002), and (4) intra-arc extension model(Lin et al., 2016). Although these models start at different times, with model 1 commencing at ca. 850 Ma, model 2 at ca. 780 Ma, model 3 at ca. 830 Ma, and model 4 at ca. 770 Ma, the controversy about the tectonic setting of the Nanhua Basin is mainly about whether the 770 Ma igneous rocks formed above a mantle superplume or were part of a continental arc system. In this paper, we document isotopic and geochemical data for ca. 770 Ma rhyolitic tuffs from Louqian Formation in Wuyi area overlying the Cathaysia Block, southern Nanhua Basin. Evidence for igneous activity in this part of the basin is rare and our results suggest an overall extensional back-arc setting that correlates with subduction along the western margin of the South China Craton. This convergent plate interaction extended from Madagascar, through the Seychelles and

northwestern India to South China along the western margin of East Gondwana.

2. Geological setting

South China consists of the Yangtze and Cathaysia blocks that were assembled along the Jiangnan Orogen in the mid-Neoproterozoic (880-830 Ma; Wang et al., 2013a; Wang et al., 2012b; Zhao, 2015). The Jiangnan Orogen comprises mainly low-grade metamorphic Neoproterozoic metasedimentary and associated igneous rocks (Fig. 2), however, the specific timing of the collision between the two continents is still controversial. Li et al. (2003a, b, 2007, 2008b) suggested that collision occurred at ca. 1.0-0.9 Ga and that the mid-Neoproterozoic (< 850 Ma) sedimentary and igneous rocks were formed in a rift setting above a mantle superplume. Others have argued that the mid-Neoproterozoic (< 850 Ma) metasedimentary units including the Fanjingshan, Lengjiaxi, Sibao groups, accumulated in an arc-back-arc basin setting corresponding to subduction between the Yangtze and Cathaysia blocks (Wang et al., 2013a). And U-Pb zircon ages from igneous units suggest magmatism continued until ca. 835 Ma, with amalgamation after this age (Wang et al., 2013b).

The amalgamated South China Craton is unconformably overlain by a middle to upper Neoproterozoic succession (Wang et al., 2003a; Wang et al., 2003b; Wang et al., 2014). The mid-Neoproterozoic (ca. 820 Ma to 715 Ma) units accumulated in the Nanhua Basin, which covered large areas of the South China Craton (Wang et al., 2003a; Wang et al., 2014).The Nanhua Basin is considered to represent a

northeasterly-trending Neoproterozoic continental rift basin (Wang and Li, 2003). Although the start time of rifting and magmatism is disput, it ended in the late Neoproterozoic (690 Ma) and was followed by a thermal sag phase for the remainder of the Neoproterozoic (Wang et al., 2003).

Lithostratigraphic units in the Nanhua Basin overlying the Yangtze Block include the Banxi, Xiajiang, Danzhou groups and their constituent formations (Figs.1 and 2, references therein), which are composed mainly of sandstone, slate, conglomerate, minor carbonate, and volcanoclastic rocks (Wang and Li, 2003). Previous geochemical and geochronological studies on units within the basin overlying the Yangtze Block have well constrained depositional ages at 820-760 Ma (Wang et al., 2003; Yin et al., 2003). Glacial/inter-glacial deposit above these units are composed of tillite /sandstone and carbonaceous shale, corresponding to the Cryogenian system (720-635 Ma) by the international Commission on Stratigraphy (Wang et al., 2013; Lan et al., 2015). Nanhua Basin rock units overlying the Cathaysia Block include the Wanquan, Mayuan, Mamianshan, Longquan, and Dikou groups, which are unconformable on the northern Wuyi domain (Fig. 2). These units are mostly composed of mica-quartz schist, actinolite schist, fine grained biotite gneiss, magnetite-bearing quartzite and marble, suggesting that their protoliths were a mixture of fine-grained siliciclastic and calcareous sedimentary rocks along with basaltic and rhyolitic volcanic rocks (Li et al., 2011; Wan et al., 2007). In the southern Wuyi domain, mid-Neoproterozoic strata are represented by the Taoxi Group and Louqian Formation (Fig. 2). The clastic materials from the Taoxi Group are mostly

from ca. 736 Ma granitoid rocks with minor Neoarchean and Paleoproterozoic rocks (Yu et al., 2005). However, the age of the Louqian Formation has been not well-established, largely reflecting a lack of study.

3. Sampling and analytical methods

3.1 Sampling and petrographic features

The Louqian Formation occurs in the Zhangdi, Xiedi and Tiechang of Changting regions County, and is characterized by low-grade metamorphic Neoproterozoic intermediate-acid volcanic rocks. The type section of the Louqian Formation is just northeast of Zhangdi village. This 2 km-long section consists of a well-bedded succession of rhyolitic and rhyodacitic tuffs and tuffaceous sandstone and mudstone, It is overlain by the Xixi Formation along a parallel unconformity, and separated from Devonian strata by S-N trending fault zones. At the type section, the Louqian Formation is subdivided into two units (Fig. 3). The lower unit starts with thick-bedded greyish yellow or green rhyolitic tuff and rhyodacitic tuff, interbedded with siliceous tuff, grading up into a 400 m thick succession of pale pink or greyish yellow rhyolitic and rhyodacitic tuffs. In the upper unit, the intensity of the felsic pyroclastic activity slightly decreases, and consists mainly of alternating rhyolitic, tuffaceous mudstone and tuffaceous sandstone, passing up into well-bedded tuffaceous mudstone, which is the top level of this type section.

Eighteen samples covering the range of lithologies were collected (Fig. 3). All samples are from fresh, non-weathered outcrops, and veins were avoided. Samples

PM01-1 and PM01-9 were chosen for zircon U-Pb isotope chronology analysis, and whole-rock geochemistry analysis including major, trace, and rare earth elements, were conducted on all eighteen samples. Field and thin-section observations show that the felsic tuffs exhibit eruptive contact relationships and flow structures (e.g., Fig. 4, Supplementary Table S1). Petrographic data indicate the samples can be classified as crystal-poor tuffs, crystal-rich tuffs and tuffaceous mudstone. Most of the samples are crystal-poor tuffs, which consist mainly 50 - 70 % devitrified glass shards and 20 % broken quartz microlites. Zircon, chlorite and apatite occur as accessory phases in the crystal-poor tuffs. The few samples of crystal-rich tuffs (PM01-1, 2, 9 and 16), consist of 40 % quartz and plagioclase. Plagioclase phenocrysts (up to 500 μm) are partly sercitized. Dark brown matrix is amorphous and consists mainly of fine-grained microlites of quartz plusdevitified glass. In some thin sections, the orientation of the quartz microlites around larger phenocrysts or lithic fragments display flow banding. Chlorite and biotite as accessory phase in the crystal-rich tuffs indicating the effects of low-grade metamorphism. Two samples (PM01-18 and PM01-19) are tuffaceous mudstone, which have obviously laminae structure consist of broken quartz, feldspar and devitrified glass shards in a clay mineral-rich matrix.

3.2 Analytical Methods

3.2.1 LA-ICP-MS U-Pb dating of zircons

Zircons were separated by conventional heavy liquid and magnetic techniques. Grains were selected under a binocular microscope at the Langfang Regional

Geophysical Survey, Hebei Province, China. Zircons are mounted in epoxy resin, sectioned and polished approximately in half, and imaged in transmitted light and by cathodoluminescence (CL) at the Beijing GeoAnalysis Co., Ltd. U-Pb datingof zircon were conducted on an Agilent 7500a laser inductively coupled plasma mass spectrometer (LA-ICP-MS) at the State Key Laboratory of Geological Processes and Mineral Resources, China University of Geosciences in Wuhan. Laser sampling was performed using an excimer laser ablation system (GeoLas 2005) with a spot size of 32 μm, and all analysis sites are marked on the CL images. Detailed operating conditions and data reduction methodologies are described by Liu et al. (2010). Off-line selection of the background and analytic integrations, as well as instrument drift correction and quantitative calibration for the U-Pb dating, were performed using ICPMSDateCal (Liu et al., 2010). Zircon 91500 was used as external standard for U-Pb dating, and was analyzed twice every five analyses. Time-dependent drift of U-Th-Pb isotopic ratios were corrected using a linear interpolation (with time) for every five analyses according to the variations of 91500. Uncertainty of preferred values for the external standard 91500 was propagated to the results of the samples. GJ-1 was analyzed as an unknown. Our measurements of 91500 and GJ-1 yielded weighted mean $^{206}Pb/^{238}U$ ages of 1062.4 ± 0.4 Ma (2 σ, MSWD = 0.051, n = 40) and 596.3 ± 5.1 (2 σ, MSWD = 2.6, n = 12), respectively, which are in good agreement with the measured isotope dilution thermal ionization mass spectrometry (ID-TIMS) $^{206}Pb/^{238}U$ ages of 1062.4 ± 0.4 and 598.5-602.7 Ma (2 σ) (Jackson et al., 2004). Concordia diagrams and weighted mean calculations were made using

Isoplot/Ex_ver3 (Ludwig, 2003). Common Pb correction was not performed as the measured ^{204}Pb signal is low and U-Pb ages are concordant or nearly concordant.

3.2.2 In-situ Lu-Hf isotope analysis of zircons

Zircon Hf isotope analyses were carried out in situ using a Neptune Plus MC-ICP-MS (Thermo Fisher Scientific, Germany) in combination with a Geolas 2005 excimer ArF laser ablation system (Lambda Physik, Göttingen, Germany) at the State Key Laboratory of Geological Processes and Mineral Resources, China University of Geosciences in Wuhan. The energy density of laser ablation was 5.3 J cm^2. A "wire" signal smoothing device is included in this laser ablation system, by which smooth signals are produced even at very low laser repetition rates down to 1 Hz (Hu et al., 2012). Details on analytical and calibration procedures are in Hu et al. (2012). Analytical spots were located close to LA-ICP-MS spots, or in the same growth domain as inferred from CL images. Reference zircons 91500 and GJ-1 were used to monitor accuracy of the interference correction during Hf analysis. Zircon 91500 yielded a $^{176}Hf/^{177}Hf$ ratio of 0.282386 ± 0.000011 (n = 14, 1 σ) compared to the recommended value of 0.282308 ± 6 (Blichert-Toft, 2008), and 0.282057 ± 0.000071 (n = 4, 1 σ) for GJ-1 compared to the recommended value of 0.282015 ± 19 (Elhlou et al., 2006). The $^{179}Hf/^{177}Hf$ and $^{173}Yb/^{171}Yb$ ratios were used to calculate the mass bias of Hf (β_{Hf}) and Yb (β_{Yb}), which were normalized to $^{179}Hf/^{177}Hf$ = 0.7325 and 173Yb/171Yb = 1.132685 (Fisher et al., 2014)using an exponential correction. Interference of ^{176}Yb on ^{176}Hf was corrected by measuring the interference-free ^{173}Yb isotope and using $^{176}Yb/^{173}Yb$ = 0.79639 (Fisher et al., 2014) to calculate $^{176}Yb/^{177}Hf$.

3.2.3 Whole-rock major and trace elements

Fresh rock samples were cleaned with deionized water, and subsequently crushed and powdered with an agate mill. The major elements of samples were determined using the ME-XRF26d method, at the ALS Chemex Company of Guangzhou, China. The prepared samples were fused with a lithium tetraborate ($Li_2B_4O_7$) and lithium metaborate ($LiBO_2$) flux and then fused to a glass bead at 1050 - 1100 °C in an automatic melting instrument. The resultant disks were analyzed using X-ray fluorescence spectrometry (XRF) for major elements. The analysis accuracy was < 2 % and the detection limits were< 0.01 %. The trace and REES were analyzed using the ME-MS81 and ME-MS62S methods, at the ALS Chemex Company of Guangzhou, China. Samples (0.200 g) was added to lithium metaborate ($LiBO_2$) flux (0.90 g), mixed well and fused in a furnace at 1000°C. The resulting melt was cooled and dissolved in 100 mL of 4 % HNO_3 / 2 % HCl_3 solution. This solution was analyzed by inductively coupled plasma - mass spectrometry (ICP-MS). In-run analytical precision for most elements was better than 3 %.

4. Results

4.1 Zircons U-Pb geochronology

Cl images of representative zircons are shown in figure5. Zircons preserved in PM01-1 and PM01-9 are colorless with well-developed oscillatory zoning and show core-rim structures under CL, which implies a magmatic origin for the zircons from two crystal-rich tuff samples. Most are euhedral, approximately 50 μm to 120 μm

long with aspect ratios of 1:1 to 2:1, and the uranium content of the zircon is 170 - 2877 ppm and the thorium content 157 - 4743 ppm, yielding Th/U ratios of 0.45 to 3.19, consistent with a magmatic origin (Belousova et al., 2002), which suggesting the zircon age of Louqian tuffs likely represents the eruption age of the magma.

A total of 41 spot analyses were undertaken on zircons from sample PM01-1, which is located at the stratigraphic base of section A-A' (Fig. 3), and a further 62 analyses were performed on sample PM01-9, located around the middle of the section. The corrected analytical results are listed in Supplementary Table S2. All PM01-1 analyses display 95% or greater concordance and fall within a narrow band of $^{206}Pb/^{238}U$ ages from 824 ± 13 to 736 ± 10 Ma with a weighted mean $^{206}Pb/^{238}U$ age of 767.58 ± 2.95 Ma (Fig. 6, MSWD = 2.41, n=41).Eighteen analyses are highly clustered on the Concordia plot and yield a weighted mean $^{206}Pb/^{238}U$ age of 770 ± 4 Ma (95% confidence, MSWD = 1.5). All 62 analyses from PM01-9 display 95% or greater concordance. Two have $^{206}Pb/^{238}U$ ages greater than 820 Ma. The remains 60 analyses fall within a narrow group of $^{206}Pb/^{238}U$ ages from 817 ± 11 to 731 ± 11 Ma, with a weighted mean $^{206}Pb/^{238}U$ age of772.6±2.45 Ma (Fig. 6, MSWD = 2.41, n=60). Twenty-five analyses are highly clustered on U-Pb Concordia diagrams and yield a weighted mean $^{206}Pb/^{238}U$ age of 771 ± 4 Ma (95% confidence, MSWD = 0.33). Collectively, the LA-ICP-MS U-Pb zircon analyses for rhyolite tuffs of the Louqian Formation suggest a ca.770 Ma crystallization age of magmatic activity, indicating that they are products of mid-Neoproterozoic magmatism.

4.2 Zircon Hf Isotope Compositions

Fourty zircons from samples PM01-1 and PM01-9 with crystallization ages of 835 Ma to 736 Ma, were analyzed for their Lu-Hf isotopic compositions and the results are listed in Supplementary Table S3.

Zircons from PM-1-1 show heterogeneous Hf-isotope compositions with varying ε_{Hf} (t) and initial $^{176}Hf/^{177}Hf$ values. Three analyses exhibit negative $\varepsilon_{Hf}(t)$ values from -3.16 to -0.23, with two-stage model ages from 1.73 Ga to 1.56 Ga, the other nine analyses have positive $\varepsilon_{Hf}(t)$ values ranging from +0.13 to +10.83 (average: +6.61 ± 1.0), with model ages of 1.55-0.99 Ga (Fig. 7).

Zircons from PM01-9 also show similar Hf-isotopes compositions. Four analyses exhibit negative $\varepsilon_{Hf}(t)$ values from -3.66 to -0.27, with two-stage model ages from 1.74 Ga to 1.54 Ga, the other 24 clustering within the range of +0.33 to +13.94, with model ages of 1.55-0.90 Ga. In summary, the ca. 770 Ma zircon grains are characterized by variable $\varepsilon_{Hf}(t)$ values, but with overall positive values suggesting derivation from juvenile crust (Fig. 7).

4.3 Whole-rock major and trace elements

Major and trace element data for the Louqian Formation samples are listed in Table 2. The majority of samples have a loss of ignition (LOI) of less than 3%. SiO_2 content range from 57.80% to 79.81%. On Harker variation diagrams most of the major elements (MgO, CaO, TiO_2 and FeO) show an inverse relationship with SiO_2 except K_2O and Na_2O, which are relatively scattered probably due to post-deposition (Fig. 8 a-f). Except for two tuffaceous mudstone samples (PM01-18 and PM01-19) with low SiO_2, Na_2O and high CIA values, the remaining sixteen crystal-poor and

crystal-rich tuff samples have similar major element characteristics and similar trace element patterns on spider diagram and REE plots. Different types of tuffs have influence on the results of geochemistry.

On an A/CNK versus A/NK plot (Maniar and Piccoli, 1989, Fig. 8g), the tuff samples display peraluminous characteristics with high $Al_2O_3/(CaO + Na_2O + K_2O)$ values. On classification diagrams based on immobile elements such as Nb/Y-Zr/Ti (Fig. 8h), the tuff samples are classified as rhyolite and rhyodacite except PM01-18 and PM01-19, which plot in the andesite field (Winchester and Floyd, 1977). The chemical index of alteration (CIA) values are very low (44.26-61.15, average 53.70), suggesting minimal alteration effects. In general, samples PM01-1 to PM01-17 from the Louqian formation are acid volcanic rocks, consistent with the findings of the field survey, showing the characteristic of high A/CNK, Zr, Nb, low Ti, Ca, Mg, low degrees of alteration and belong to the magnesian and peraluminous series. PM01-18 and PM01-19 have lower SiO_2, Na_2O, but much higher CIA values (Table. 5), which could be the result of post-crystallization alteration.

All samples (include crystal-poor tuffs, crystal-rich tuffs and tuffaceous mudstone) have high ΣREE contents, ranging from 175.03 to 437.43, with an average of 277.95 ppm. On the chondrite normalized REE plots (Boynton, 1984, Fig. 9a), all the samples show strong enrichment of light rare earth elements (LREEs) and a weakly fractionated flat pattern of heavy rare earth elements (HREEs). The average LREEs/ HREEs is 4.55, the average $(La/Yb)_n$ is 14.28, the average $(La/Sm)_n$ is 5.31, and the average $(Gd/Yb)_n$ is 1.66. All of the samples show a significant negative Eu

anomaly, and three samples show a slightly negative Ce anomaly, with the former indicative of crystal fractionation of plagioclase (Nagasawa and Schnetzler, 1971). On the primitive mantle normalized trace elements spider diagram (Fig. 9b), all samples show enrichment in large ion lithophile elements (LILEs) (e.g. Rb, Th, U and REEs), strong depletion in high field strength elements (HFSEs) (e.g. Nb, Ta, Ti and P), and no positive anomalies of Zr and Hf. Slightly negative Ba anomalies and large Sr anomalies are also observed (Fig. 9b).

Comparison of the samples from the Louqian Formation with contemporaneous (800-750 Ma) felsic rocks in central South China, in the vicinity of the Jiangnan Orogen (Li et al., 2018b; Wang et al., 2010;Wang et al., 2013;Yao et al., 2014a;Zheng et al., 2008), and from the western and northern margin of South China (Lin et al., 2016; Luo et al., 2018; Wang et al., 2008; Zhou et al., 2007), indicate a number of similarities. These include major element compositions with the A-type igneous rocks overlying the eastern Jiangnan Orogen (e.g., SiO_2, Na_2O, CaO and FeO values), with all displaying peraluminious compositions and affinities to the A_2-type magma series (figs 8, 9 and 11). REE, Zr, Ti and Eu values are also similar to samples overlying the eastern Jiangnan Orogen (Fig. 9). In contrast, the geochemical character of the Louqian Formation tuffs differs from contemporaneous and nearby igneous rocks in the northern Wuyi domain of Cathaysia Block, which exhibit higher Eu, Ta, Zr and Hf, and lower Y.

5. Discussion

5.1 Reconstruction of mid-Neoproterozoic stratigraphy in eastern South China.

Strata of the Nanhua Basin are disconformably overlain Louqian Formation by upper Neoproterozoic rocks(ca. 645 - 545 Ma) of the the Louziba, Nanyan, Huanglian and Xixi formations (Qi et al., 2018). Magmatic zircons in rhyolitic and rhyodacitic tuffs of the Louqian Formation, that unconformably overlie the Wuyi domain of the Cathaysia Block yield U-Pb ages of ca. 770 Ma. This provides a maximum depositional age for the overlying Xixi Formation, and it is consistent with the youngest detrital zircon from the Xixi Formation yielding a concordant age of 636 ± 11 Ma (Qi et al., 2018, Fig. 2), and with the micro-fossil acritarchs *Micurhystridium* sp., and *Leiominuscula* sp. in late Neoproterozoic strata from the eastern and central regions of the South China Craton. Tuff units within the measured section of the Louqian Formation reach up to 400m and contain crystal fragment up to 800 μm (Fig. 4), which together with the ubiquitous presence of tuffs through the formation (Fig. 3) suggests derivation from a relatively proximal magmatic source.

Previous studies of the mid-Neoproterozoic stratigraphy in eastern South Chinahave been well studied based on a great deal of zircon U-Pb ages (Chen et al., 2018a; Wan et al., 2007; Wang et al., 2010; Zhou et al., 2007; Wang et al., 2012a; Zheng et al., 2008). The ca. 770 Ma age for the rhyolite tuffs provide supplemental stratigraphy information about Louqian Formationand indicate correlations with the Wanquan, Mamianshan, Longquan and Dikou groups in the southeastern Nanhua Basin, and with the Ejiaao, Qingshuijiang, Sanmenjie, Shangshu, Puling and Jingtan formations in the northwestern Nanhua Basin. Apart from the Louqian Formation, the

units in the southeastern Nanhua Basin were strongly deformed and metamorphosed during mid-Paleozoic orogenic activity which suggest that the Louqian Formation lay within a semi-rigid block, isolated from the more intense effects of mid-Paleozoic orogenesis (Zhao et al., 2015; Chen et al., 2018a).

5.2 Origin of the Louqian rhyolitic tuffs

Petrologic and geochemical characteristics of the Louqian tuffs exhibit A-type affinities; for example, high SiO_2, Ga, Th, Nb, Y, REE, low CaO, Sr, Ti and Ba content, enriched LREE and flat HREE pattern, and accentuated negative Eu anomalies(Loiselle, 1979; Wang et al., 2010). Most of the analyzed samples are characterized by a ratio of 10000×Ga/Al > 2.6, of Zr+Nb+Ce+Y> 350 μg/g, and on the discrimination diagrams of 10000×Ga/Al versus Zr+Nb+Ce+Y and 10000×Ga/Al versus $(Na_2O+K_2O)/CaO$, the samples largely fall in the A-type field. Using the bulk-rock compositions and equation proposed by Watson and Harrison (1983), we calculated the zircon saturation temperatures (T_{Zr}) of these rocks. The results show that the calculated T_{Zr} ranges from 803 °C to 945 °Cwith an average of 852 °C (Fig. 10e; Supplementary Table S2), indicating crystallization from magmas at higher temperatures than rocks of I-type affinity but consistent with an A-type origin (Bonin, 2007; Clemens et al., 1986; Watson and Harrison, 1983). A-type rocks have been classified into A_1-type (or anorogenic) and A_2-type (or post-collisional) by Eby (1992). The Louqian rhyolitic tuff as well as other ca.780 Ma A-type rocks in the Nanhua basin overlying the eastern Jiangnan Orogen mostly plot in the A_2-type field on the Y/Nb versus Rb/Nb and Nb versus Y versus Ce diagrams..

A-type rocks can be formed through a number of magmatic processes, including partial melting of either the mantle or the crust, fractional crystallization of mantle melts, AFC processes (crustal assimilation plus fractional crystallization) and magma mixing between basaltic and crustal melts (Clemens et al., 1986; Collins et al., 1982; Eby, 1992; Wang et al., 2010; Wu et al., 2002). Other studies of the contemporaneous felsic rocks from the northwestern parts of Nanhua Basin, includingthe Shangshu rhyolite, Jingtan dacite, Daolinshan granite and Shi'ershan granite, have suggested a number of possible origins. These include partial melting of early Neoproterozoic juvenile crustal materials, underplating of mafic tholeiitic magmas into the lower crust, or fractional crystallization of basaltic magmas (Li et al., 2018b; Li et al., 2008a; Wang et al., 2010; Wang et al., 2012b; Zheng et al., 2008). No geological and petrographic evidence has been found for magma mixing and mingling. In addition, our samples have T_{DM}(Hf) values similar to contemporary mafic igneous rocks in the Nanhua Basin, and lack inherited zircons (Fig. 3), which argue against crustal assimilation or magma mixing in the petrogenesis of the Louqian tuffs. Both anatexis of the continental crust and the fractional crystallization of mafic-andesite can generate high siliceous magma. The peraluminous characteristics of the analyzed samples (Fig. 8g), and Nb/Ta ratios (12.42-16.86), which are conspicuously lower than the mantle average value (60.0) (Li, 1976), suggest derivation from partial melting of variable crustal components.

Zircons from the Lougian Formation samples exhibit depleted initial $^{176}Hf/^{177}Hf$ ratios (0.282225-0.282712), high $\varepsilon_{Hf}(t)$ (with average +4.56) values, and low T_{DM}(Hf)

ages (with average of 1.16 Ga). These values are close to contemporaneous (ca.770 Ma) igneous rocks found elsewhere in the Nanhua basin, for example, Shi'ershan granites (with average +5.27, 1.15 Ga, Wang et al., 2013b; Zheng et al., 2008), Jingtan volcanic rocks (with average of +7.1, 1.10 Ga, Li et al., 2018b), and Qingshuijiang tuff (with average +5.33, 1.37Ga, Wang et al., 2012a)(Fig. 7). The overall positive $\varepsilon_{Hf}(t)$ values and low T_{DM} ages for Lougian zircons indicate the source region is mainly composed of relatively juvenile crust largely generated in the Mesoproterozoic to early Neoproterozoic (Fig. 7). Eight zircons have relatively high $\varepsilon_{Hf}(t)$ (+8.97 to +13.94) and young $T_{DM}(Hf)$ ages (0.98 to 0.79 Ga), thus the products of contemporary arc (like Panxi-Hannan arc or Shuangxiwu arc) materials may also have been incorporated into the source region. Combined with the similarities in geochemical character between Louqian Formation and contemporaneous (800-750 Ma) felsic rocks in central South China (Figs. 7, 8, 9, 10), our tuff samples were possibly ejected from volcanoes in the eastern Jiangnan Orogen.

5.3 Tectonic significance

In the South China Craton, the mid-Neoproterozoic (ca. 830-730) is a period of continental extension resulting in accumulation of a siliciclastic succession that contain bimodal igneous rocks in the lower parts (Li et al., 2018b; Li et al., 2008a; Li et al., 2003; Wang et al., 2010; Wu et al., 200b; Yao et al., 2014a; Zheng et al., 2008; Zhou et al., 2007). These Neoproterozoic strata are inferred to have accumulated within a rift basin, termed the Nanhua Basin.

Different models have been proposed for the geodynamic setting of the basin during mid-Neoproterozoic based on data from the central parts of the basin, including plume-rift model, plume-rift model, slab-arc model and intra-arc extension model (Li et al., 2003; Lin et al., 2016; Wang et al., 2007; Yao et al., 2014b; Zheng et al., 2008; Zheng et al., 2007; Zhou et al., 2002;7 Zhou et al., 2006).. The slab-arc modal suggests that the third argues the arc magmatism occurred around Yangtze Block at ca.770 Ma.

Our analyzed samples from the southeastern part of the Nanhua basin, along with the previous studies on felsic rocks from further west indicate A-type and strong arc-affinities (Figs. 11). Such A-type felsic rocks are spatially and temporally associated with basalts or mafic dykes in central South China (Fig. 1b), thus possibly representing a bimodal igneous suite, typical of rock assemblages in an extensional setting (Li et al., 2011; Li et al., 2008a; Li et al., 2002). An island-arc origin is suggested for some of contemporaneous magmatic rocks, which can be interpreted either as the product of partial melting of previous arc rocks during the development of the Nanhua basin (first two models above), or form both previous and contemporaneous arcs (third model). Many researchers have considered that the A-type and arc-affinities observed in some volcanic rocks may be inherited from former subduction event (Zheng 2008 et al., Li et al., 2008a), and we agree that plume-rift modal cannot be ruled out solely on the basis of previous geochemistry. However, the relatively young T_{DM}(Hf) ages (the youngest age is 0.79 Ga) and the presence of contemporaneous arc magmatism along the western and northern margin

of South China (Panxi-Hannan Belt) (Dong et al., 2012; Zhao and Zhou, 2007; Zhou et al., 2002), supports an overall contemporaneous supra-subduction zone, back arc setting for the Nanhua Basin. Also, broad geological relationships between the magmatic activity, including its distribution across South China (beyond the Nanhua Basin) and with inferred consanguineous blocks in regions such as India, ague against a plume rift model (Xu et al., 2013; Wang et al., 2012c; Qi e al., 2018). The felsic composition of the igneous source rocks for the Nanhua sequences and the detrital record of the late Cryogenian and Ediacaran strata in the Cathaysia Block do not support development in association with mantle plume located between western Laurentia and Australia (Wang et al., 2012c; Qi et al., 2018). In addition, stratigraphic, structural, geochemical and geochronological from sedimentary rocks in South China (Shu et al., 2015; Shu et al., 2014; Xu and Du, 2018; Xu et al., 2016) do not comply with the final model that oceanic crust was emplaced in the Nanhua Basin during mid-Neoproterozoic. Our data from the southeastern part of the basin and their overall lithotectonic correlations with strata further west in the basin argue against these successions accumulating on opposite sides of a closing ocean as proposed by the fourth model.

The Panxi-Hannan Belt had a protracted record of subduction-related magmatism (from 860 to 730 Ma, Dong et al., 2012; Li et al., 2018a) and took place in a complex arc-trench-basin system along the western and northern margins of South China (Zhao et al., 2011). A inferred slab breakoff event associated with this subduction zone is proposed to have triggered large igneous province in NW India

contains asthenosphere-derived MORB and OIB-like basalts (Wang et al., 2017; Zhao et al., 2018). And the mid-late Neoproterozoic, rift-related igneous and sedimentary rocks within Nanhua Basinhave the similar subduction-induced extension record with the coeval basins in NW India (such as the Punagarh and Sindreth sequences in the MIS, the Jaunsar-Simla and Blaini sequences in the Lesser Himalaya) (Wang et al., 2018). This subduction zone lies along strike from contemporaneous magmatic activity extending from Madagascar, into the Seychelles and on through northwestern India (Fig.12b; Archibald et al., 2017; Ashwal et al., 2013; Rao et al., 2014; Thomas et al., 2009; Wang et al., 2017; Wang et al., 2018). Thus, a peripheral setting for South China adjacent to India during mid-Neoproterozoic has been proposed (Cawood et al., 2013; 2018; Hoffmann et al., 2011; Merdith 2017) (Fig. 12a), which is consistent with our back arc model (Fig.12c). Assuming that the subduction continued along the western margin of Yangtze and its along strike extensions until 730 Ma, it can be inferred that ca. 770 Ma magmatism within the South China Craton overlaps with the mid-Neoproterozoic magmatic arcs that formed during the destruction of Mozambique Ocean floor prior to the final assembly of Gondwana.

6. Conclusions

New zircon U-Pb dating results yelding an age of ca.770 Ma, are documented for rhyolite tuffs in the Louqian Formation in the eastern South China Craton. Geochemical and Hf-isotopic data suggest that the felsic volcanic rocks are derived from partial melting of Mesoproterozoic, early Neoproterozoic and contemporary

juvenile crust materials, which were broadly synchronous with widespread magmatism in the Nanhua Basin. The presence of contemporaneous arc magmatism along the western margin of South China and extending into along strike continental fragments in western India, Madagascar, and the Seychelles supports an overall back arc setting. Thus, the A-type and arc-affinities of the volcanic rocks in the Nanhua Basin support the hypothesis that South China lay adjacent to India in a peripheral setting of Rodinia.

Acknowledgments

This work was supported by the National Natural Science Foundation of China (Grant No. 41772106 and 41472086) and by the Australian Research Council (GrantFL160100168). We would like to thank Hu Huang and Lisha Hu for beneficial discussions, and Yahui Zang, Hangchuan Zhang and Zukun Zhang from our group and Ciluan Lin from the Regional Geological Survey of Fujian Province for their help during fieldwork. Zhaochu Hu is thanked for help with zircon U-Pb and Hf isotope analyses. The manuscript benefitted from the comments from the editor and two anonymous reviewers.

References

Archibald, D. B., Collins, A. S., Foden, J. D., and Razakamanana, T., 2017. Tonian arc magmatism in central Madagascar: the petrogenesis of the Imorona-Itsindro Suite. J. Geol. 125, 271-297.

Ashwal, L. D., Solanki, A. M., Pandit, M. K., Corfu, F., Hendriks, B. W. H., Burke, K., and Torsvik, T. H., 2013. Geochronology and geochemistry of Neoproterozoic Mt. Abu granitoids, NW India: Regional correlation and implications for Rodinia paleogeography. Precambr. Res. 236, 265-281.

Belousova, E., Griffin, W., O'Reilly, S. Y., and Fisher, N., 2002. Igneous zircon: trace element composition as an indicator of source rock type. Contrib. Mineral. Petr. 143, 602-622.

Blichert-Toft, J., 2008. The Hf isotopic composition of zircon reference material 91500. Chem. Geol. 253, 252-257.

Bonin, B., 2007. A-type granites and related rocks: Evolution of a concept, problems and prospects. Lithos 97, 1-29.

Boynton, W., 1984, Cosmochemistry of the earth elements: meteorite studies. Rare Earth Element Geochmistry.

Cawood, A., Wang, Y., Xu, Y., and Zhao, G., 2013. Locating South China in Rodinia and Gondwana: A fragment of greater India lithosphere? Geology 41, 903-906.

Cawood, A., Zhao, G., Yao, J., Wang, W., Xu, Y., and Wang, Y., 2018. Reconstructing South China in Phanerozoic and Precambrian supercontinents. Earth-Sci Rev.

Chen, C.-H., Lee, C.-Y., Liu, Y.-H., Xiang, H., Zeng, W., and Zhou, H.-W., 2018a, Precambrian protoliths and Phanerozoic overprinting on the Wuyishan terrain (South China): New evidence from a combination of LA-ICPMS zircon and EMP monazite geochronology.

Precambr. Res. 307, 229-254.

Chen, X., Wang, X.-L., Wang, D., and Shu, X.-J., 2018b, Contrasting mantle-crust melting processes within orogenic belts: Implications from two episodes of mafic magmatism in the western segment of the Neoproterozoic Jiangnan Orogen in South China. Precambr. Res. 309, 123-137.

Clemens, J. D., Holloway, J. R., and White, A. J. R., 1986, Origin of an A-type granite; experimental constraints: American Mineralogist 7, 317-324.

Collins, W. J., Beams, S. D., White, A. J. R., and Chappell, B. W., 1982, Nature and origin of A-type granites with particular reference to southeastern Australia: Contributions to Mineralogy & Petrology 80, 189-200.

Condon, D., Zhu, M. Y., Bowring, S., Wang, W., Yang, A. H., Jin, Y. G., 2005, U-Pb ages from the neoproterozoic Doushantuo Formation, China: Science 308, 95-98.

Dong, Y., Liu, X., Santosh, M., Chen, Q., Zhang, X., Li, W., He, D., and Zhang, G., 2012. Neoproterozoic accretionary tectonics along the northwestern margin of the Yangtze Block, China: Constraints from zircon U–Pb geochronology and geochemistry. Precambr. Res. 196-197, 247-274.

Drummond, M. S., Defant, M. J., and Kepezhinskas, K., 2011. Petrogenesis of slab-derived trondhjemite–tonalite–dacite/adakite magmas: Transactions of the Royal Society of Edinburgh. Earth Sci.s 87, 205-215.

Eby, G. N., 1992, Chemical subdivision of A-type granitoids: Petrogenesis and tectonic implications. Geology 20, 641.

Elhlou, S., Belousova, E., Griffin, W. L., Pearson, N., and O'Reilly, S. Y., 2006. Trace element and

isotopic composition of GJ-red zircon standard by laser ablation: Geochimica et Cosmochimica Acta 70, . A158.

Fisher, C. M., Vervoort, J. D., and Hanchar, J. M., 2014. Guidelines for reporting zircon Hf isotopic data by LA-MC-ICPMS and potential pitfalls in the interpretation of these data. Chem. Geol. 363, 125-133.

Gorton, M. P., and Schandl, E. S., 2000. From continents to island arcs: a geochemical index of tectonic setting for arc-related and within-plate felsic to intermediate volcanic rocks: The Canadian Mineralogist 38, 1065-1073.

Hu, Z., Liu, Y., Gao, S., Liu, W., Zhang, W., Tong, X., Lin, L., Zong, K., Li, M., Chen, H., Zhou, L., and Yang, L., 2012. Improved in situ Hf isotope ratio analysis of zircon using newly designed X skimmer cone and jet sample cone in combination with the addition of nitrogen by laser ablation multiple collector ICP-MS: Journal of Analytical Atomic Spectrometry 27, 1391.

Jackson, S. E., Pearson, N. J., Griffin, W. L., and Belousova, E. A., 2004. The application of laser ablation-inductively coupled plasma-mass spectrometry to in situ U–Pb zircon geochronology. Chem. Geol. 211, 47-69.

Li, J. Y., Wang, X. L., Gu, Z. D., 2018a. Petrogenesis of the Jiaoziding granitoids and associated basaltic porphyries: Implications for extensive early Neoproterozoic arc magmatism in western Yangtze Block. Lithos 296-299, 547-562.

Li, L., Lin, S., Xing, G., Jiang, Y., and Xia, X., 2018c. Geochronology and geochemistry of volcanic rocks from the Jingtan Formation in the eastern Jiangnan orogen, South China: Constraints on petrogenesis and tectonic implications. Precambr. Res. 309, 166-180.

Li, T., 1976, Chemical element abundances in the earth and it's major shells: Geochimica 3, 167-174.

Li, W. X., Li, X. H., and Li, Z. X., 2011. Ca. 850 Ma bimodal volcanic rocks in northeastern Jiangxi Province, South China: Initial extension during the breakup of Rodinia?. Am. J. Sci. 310, 951-980.

Li, X.-H., Li, W.-X., Li, Z.-X., and Liu, Y., 2008a. 850–790 Ma bimodal volcanic and intrusive rocks in northern Zhejiang, South China: A major episode of continental rift magmatism during the breakup of Rodinia. Lithos 102, 341-357.

Li, X.-H., Li, Z.-X., Ge, W., Zhou, H., Li, W., Liu, Y., and Wingate, M. T., 2003a. Neoproterozoic granitoids in South China: crustal melting above a mantle plume at ca. 825 Ma?. Precambr. Res. 122, 45-83.

Li, X.-H., Li, Z.-X., Zhou, H., Liu, Y., and Kinny, D., 2002. U–Pb zircon geochronology, geochemistry and Nd isotopic study of Neoproterozoic bimodal volcanic rocks in the Kangdian Rift of South China: implications for the initial rifting of Rodinia. Precambr. Res. 113, 135-154.

Li, Z. X., Bogdanova, S. V., Collins, A. S., Davidson, A., De Waele, B., Ernst, R. E., Fitzsimons, I. C. W., Fuck, R. A., Gladkochub, D. P., Jacobs, J., Karlstrom, K. E., Lu, S., Natapov, L. M., Pease, V., Pisarevsky, S. A., Thrane, K., and Vernikovsky, V., 2008b. Assembly, configuration, and break-up history of Rodinia: A synthesis. Precambr. Res. 160, 179-210.

Li, Z. X., Li, X. H., Kinny, D., and Wang, J., 1999. The breakup of Rodinia: did it start with a mantle plume beneath South China? Earth. Planet. Sc. Lett. 173, 171-181.

Lin, M., Peng, S., Jiang, X., Polat, A., Kusky, T., Wang, Q., and Deng, H., 2016. Geochemistry,

petrogenesis and tectonic setting of Neoproterozoic mafic–ultramafic rocks from the western Jiangnan orogen, South China. Gondwana Res. 35, 338-356.

Liu, Y., Gao, S., Hu, Z., Gao, C., Zong, K., Wang, D., 2010. Continental and Oceanic Crust Recycling-induced Melt-Peridotite Interactions in the Trans-North China Orogen: U-Pb Dating, Hf Isotopes and Trace Elements in Zircons from Mantle Xenoliths. J. Petrol. 51, 537-571.

Loiselle, M., Characteristics and origin of anorogenic granites, in Proceedings Geological Society of America Abstracts with Programs, 11, 468.

Ludwig, K., 2003. Users manual for ISOPLOT/EX, version 3. A geochronological toolkit for Microsoft Excel. Berkeley Geochronology Center Special Publication, 4.

Luo, B. J., Liu, R., Zhang, H. F., Zhao, J. H., Yang, H., Xu, W. C., Guo, L., Zhang, L., Tao, L., Pan, F., Wang, W., Gao, Z., and Shao, H., 2018. Neoproterozoic continental back-arc rift development in the Northwestern Yangtze Block: Evidence from the Hannan intrusive magmatism. Gondwana Res. 59, 27-42.

Maniar, D., and Piccoli, M., 1989. Tectonic discrimination of granitoids. Geol. Soc. Am. Bull. 101, 635-643.

Merdith, A. S., Williams, S. E., Müller, R. D., and Collins, A. S., 2017. Kinematic constraints on the Rodinia to Gondwana transition. Precambr. Res. 299, 132-150.

Nagasawa, H., and Schnetzler, C. C., 1971.Partitioning of rare earth, alkali and alkaline earth elements between phenocrysts and acidic igneous magma: Geochimica Et Cosmochimica Acta 35, 953-968.

Pearce, J. A., Harris, N. B., and Tindle, A. G., 1984. Trace element discrimination diagrams for the

tectonic interpretation of granitic rocks. J. Petrol. 25, 956-983.

Powell, C. M., Li, Z. X., Mcelhinny, M. W., Meert, J. G. Park, J.K., 1993. Paleomagnetic constraints on timing of the Neoproterozoic breakup of Rodinia and the Cambrian formation of Gondwana. Geology 21, . 889-892.

Qi, L., Xu, Y., Cawood, P.A., Du, Y., 2018. Reconstructing Cryogenian to Ediacaran successions and paleogeography of the South China Block. Precambr. Res. 314, 452-467.

Rao, C. V. D., Santosh, M., and Zhang, S.-H., 2014. Neoproterozoic massif-type anorthosites and related magmatic suites from the Eastern Ghats Belt, India: Implications for slab window magmatism at the terminal stage of collisional orogeny. Precambr. Res. 240, 60-78.

Shu, L., Wang, B., Cawood, A., Santosh, M., and Xu, Z., 2015. Early Paleozoic and Early Mesozoic intraplate tectonic and magmatic events in the Cathaysia Block, South China. Tectonics 34, 1600-1621.

Shu, L. S., Jahn, B. M., Charvet, J., Santosh, M., Wang, B., Xu, X. S., and Jiang, S. Y., 2014. Early Paleozoic depositional environment and intraplate tectono-magmatism in the Cathaysia Block (South China): Evidence from stratigraphic, structural, geochemical and geochronological investigations. Am. J. Sci. 314, 154-186.

Sun, S.-S., and McDonough, W.-s., 1989. Chemical and isotopic systematics of oceanic basalts: implications for mantle composition and processes: Geological Society, London, Special Publications 42, 313-345.

Thomas, R. J., Waele, B. D., Schofield, D. I., Goodenough, K. M., Horstwood, M., Tucker, R., Bauer, W., Annells, R., Howard, K., and Walsh, G., 2009. Geological evolution of the Neoproterozoic Bemarivo Belt, northern Madagascar. Precambr. Res. 172, 279-300.

Wan, Y., Liu, D., Xu, M., Zhuang, J., Song, B., Shi, Y., and Du, L., 2007. SHRIMP U–Pb zircon geochronology and geochemistry of metavolcanic and metasedimentary rocks in Northwestern Fujian, Cathaysia block, China: Tectonic implications and the need to redefine lithostratigraphic units. Gondwana Res. 12, 166-183.

Wang, J., Li, X., Duan, T., Liu, D., Song, B., Li, Z., and Gao, Y., 2003a. History of Neoproterozoic rift basins in South China: implications for Rodinia break-up. Precambr. Res. 122, 141-158.

Wang, J., Zhou, X., Deng, Q., Fu, X., Duan, T., and Guo, X., 2014. Sedimentary successions and the onset of the Neoproterozoic Jiangnan sub-basin in the Nanhua rift, South China. Int. J. Earch Sci. 104, 521-539.

Wang, Q., Wyman, D. A., Li, Z.-X., Bao, Z.-W., Zhao, Z.-H., Wang, Y.-X., Jian, P., Yang, Y.-H., and Chen, L.-L., 2010. Petrology, geochronology and geochemistry of ca. 780Ma A-type granites in South China: Petrogenesis and implications for crustal growth during the breakup of the supercontinent Rodinia. Precambr. Res. 178, 185-208.

Wang, W., Cawood, A., Zhou, M. F., Pandit, M. K., Xia, X. P., and Zhao, J. H., 2017. Low - δ18O Rhyolites From the Malani Igneous Suite: A Positive Test for South China and NW India Linkage in Rodinia. Geophys Res. Lett. 44, 298-305.

Wang, W., Pandit, M. K., Zhao, J.-H., Chen, W.-T., and Zheng, J.-P., 2018. Slab break-off triggered lithosphere - asthenosphere interaction at a convergent margin: The Neoproterozoic bimodal magmatism in NW India. Lithos 296-299, 281-296.

Wang, W., Zhou, M.-F., Yan, D.-P., Li, L., and Malpas, J., 2013a. Detrital zircon record of Neoproterozoic active-margin sedimentation in the eastern Jiangnan Orogen, South China. Precambr. Res. 235, 1-19.

Wang, W., Zhou, M.-F., 2012c. Sedimentary records of the Yangtze Block (South China) and their correlation with equivalent Neoproterozoic sequences on adjacent continents. Sedimentary Geology. 265-266, 126-142.

Wang, X.-C., Li, X.-h., Li, Z.-X., Li, Q.-l., Tang, G.-Q., Gao, Y.-Y., Zhang, Q.-R., and Liu, Y., 2012a. Episodic Precambrian crust growth: Evidence from U–Pb ages and Hf–O isotopes of zircon in the Nanhua Basin, central South China. Precambr. Res. 222-223, 386-403.

Wang, X.-L., Shu, L.-S., Xing, G.-F., Zhou, J.-C., Tang, M., Shu, X.-J., Qi, L., and Hu, Y.-H., 2012b. Post-orogenic extension in the eastern part of the Jiangnan orogen: Evidence from ca 800–760Ma volcanic rocks. Precambr. Res. 222-223, 404-423.

Wang, X.-L., Zhou, J.-C., Wan, Y.-S., Kitajima, K., Wang, D., Bonamici, C., Qiu, J.-S., and Sun, T., 2013b. Magmatic evolution and crustal recycling for Neoproterozoic strongly peraluminous granitoids from southern China: Hf and O isotopes in zircon. Earth. Planet. Sc. Lett. 366, 71-82.

Wang, X.-L., Zhao, G. C..Zhou, J.-C., Liu, Y. Hu, J. 2008. Geochronology and Hf isotopes of zircon from volcanic rocks of the Shuangqiaoshan Group, South China: Implications for the Neoproterozoic tectonic evolution of the eastern Jiangnan orogen. Gondwana Research 14, 355-367.

Wang, Y., Zhang, A., Cawood, A., Fan, W., Xu, J., Zhang, G., and Zhang, Y., 2013c. Geochronological, geochemical and Nd–Hf–Os isotopic fingerprinting of an early Neoproterozoic arc–back-arc system in South China and its accretionary assembly along the margin of Rodinia. Precambr. Res. 231, 343-371.

Watson, E. B., and Harrison, T. M., 1983. Zircon saturation revisited: temperature and

composition effects in a variety of crustal magma types. Earth. Planet. Sc. Lett. 64, 295-304.

Whalen, J. B., Currie, K. L., and Chappell, B. W., 1987,. A-type granites: geochemical characteristics, discrimination and petrogenesis. Contrib. Mineral. Petr. 95, 407-419.

Winchester, J., and Floyd, P., 1977. Geochemical discrimination of different magma series and their differentiation products using immobile elements. Chem. Geol. 20, 325-343.

Wu, F. Y., Sun, D. Y., Li, H., Jahn, B. M., and Wilde, S., 2002. A-type granites in northeastern China: age and geochemical constraints on their petrogenesis. Chem. Geol. 187, 143-173.

Wu, R.-X., Zheng, Y.-F., Wu, Y.-B., Zhao, Z.-F., Zhang, S.-B., Liu, X., and Wu, F.-Y., 2006. Reworking of juvenile crust: Element and isotope evidence from Neoproterozoic granodiorite in South China. Precambr. Res. 146, 179-212.

Xu, X., O'Reilly, S. Y., Griffin, W. L., Wang, X., Pearson, N. J., and He, Z., 2007. The crust of Cathaysia: Age, assembly and reworking of two terranes. Precambr. Res. 158, 51-78.

Xu, Y. J., Cawood, P.A., Du, Y.S., Hu, L.S., Yu, W.C., Zhu, Y.H., Li, W.C., 2013. Linking south China to northern Australia and India on the margin of Gondwana: Constraints from detrital zircon U-Pb and Hf isotopes in Cambrian strata. Tectonics 32, 1547-1558.

Xu, Y., and Du, Y., 2018. From Periphery Collision to Intraplate Orogeny:Early Paleozoic Orogenesis in Southeastern Part of South China. Earth Sci. 43, 333-353

Xu, Y. J., Cawood, A., and Du, Y. S., 2016. Intraplate orogenesis in response to Gondwana assembly: Kwangsian Orogeny, South China. Am. J. Sci. 316, 329-362.

Yao, J., Shu, L., and Santosh, M., 2014a. Neoproterozoic arc-trench system and breakup of the South China Craton: Constraints from N-MORB type and arc-related mafic rocks, and anorogenic granite in the Jiangnan orogenic belt. Precambr. Res. 247, 187-207.

Yao, W. H., Li, Z. X., Li, W. X., Li, X. H., and Yang, J. H., 2014b. From Rodinia to Gondwanaland: A tale of detrital zircon provenance analyses from the southern Nanhua Basin, South China. Am. J. Sci. 314, 278-313.

Yu, J., Zhou, X., O'Reilly, Y. S., Zhao, L., Griffin, W. L., Wang, L., Chen, X., 2005. Formation history and protolith characteristics of granulite facies metamorphic rock in Central Cathaysia deduced from U-Pb and Lu-Hf isotopic studies of single zircon grains. Chinese Sci. Bull. 50, 13-22.

Zhao, G., 2015. Jiangnan Orogen in South China: Developing from divergent double subduction. Gondwana Res. 27, 1173-1180.

Zhao, G., and Cawood, A., 2012. Precambrian geology of China. Precambr. Res. 222-223, 13-54.

Zhao, J.-H., Zhou, M.-F., Yan, D.-P., Yang, Y.-H., and Sun, M., 2008. Zircon Lu–Hf isotopic constraints on Neoproterozoic subduction-related crustal growth along the western margin of the Yangtze Block, South China. Precambr. Res. 163, 189-209.

Zhao, J.-H., Li, Q.-W., Liu, H., Wang, W., 2018. Neoproterozoic magmatism in the western and northern margins of the Yangtze Block (South China) controlled by slab subduction and subduction-transform-edge-propagator. Earth-Sci Rev.

Zheng, Y.-F., Wu, R.-X., Wu, Y.-B., Zhang, S.-B., Yuan, H., and Wu, F.-Y., 2008. Rift melting of juvenile arc-derived crust: Geochemical evidence from Neoproterozoic volcanic and granitic rocks in the Jiangnan Orogen, South China. Precambr. Res. 163, 351-383.

Zheng, Y.-F., Zhang, S.-B., Zhao, Z.-F., Wu, Y.-B., Li, X., Li, Z., and Wu, F.-Y., 2007. Contrasting zircon Hf and O isotopes in the two episodes of Neoproterozoic granitoids in South China: implications for growth and reworking of continental crust. Lithos 96, 127-150.

Zhou, J., Li, X.-H., Ge, W., and Li, Z.-X., 2007. Age and origin of middle Neoproterozoic mafic magmatism in southern Yangtze Block and relevance to the break-up of Rodinia. Gondwana Res. 12, 184-197.

Zhou, M.-F., Yan, D.-P., Kennedy, A. K., Li, Y., and Ding, J., 2002. SHRIMP U–Pb zircon geochronological and geochemical evidence for Neoproterozoic arc-magmatism along the western margin of the Yangtze Block, South China. Earth. Planet. Sc. Lett. 196, 51-67.

Zhou, M. F., Yan, D. P., Wang, C. L., Qi, L., and Kennedy, A., 2006b. Subduction-related origin of the 750Ma Xuelongbao adakitic complex (Sichuan Province, China): Implications for the tectonic setting of the giant Neoproterozoic magmatic event in South China. Earth. Planet. Sc. Lett. 248, 286-300.

Fig. 1. (a) Tectonic outline of east Eurasia (modified from Cawood et al., 2018), and (b) simplified geological map of the South China Craton showing the main tectono-stratigraphic units(modified from Xu et al., 2013 and Cawood et al., 2018). Sources of age data from Central South China Craton for Neoproterozoic volcanic rocks given in Table1, sources of age data from western and northern South China Craton see Yang et al. (2006).

Fig. 2. Stratigraphic correlation chart for late Neoproterozoic to early Paleozoic rock units of the South China Craton. Radiometric ages are from Condon et al. (2005), Lan et al. (2017), Lan et al. (2015), Lan et al. (2014), Wang et al. (2013c), Yu et al. (2005), Zhang et al. (2008), and Zhou et al. (2004), Wan et al. (2007).

Fig. 3. Simplified geological map and sample locations in the Changting area, southern Wuyi domain.

Fig. 4. Field (a, c, e, g) and microscope (b, d, f, h) photographs for the rhyolitic tuff of the Louqian Formation in the eastern South China.

Fig. 5. CL images of representative zircons showing main types of internal structures from PM01-1 and PM01-9 samples. Red circles show location of U-Pb analysis spots, and white circles denote Lu-Hf analysis spots.

Fig. 6. U-Pb Concordia diagrams of zircon analyses.

Fig. 7. Summary of $\varepsilon_{Hf}(t)$ data for zircon grains from the studied sedimentary rocks within 5% of Concordia for the analyzed samples.Comparative data from the Shi'ershan granite and Jingtan felsic volcanic rocks (Zheng et al., 2008; Wang et al.,2013b), Daolinshan granite (Wang et al., 2010; Yao et al., 2014a), Mafic rocks on western Yangtze side of Nanhua Basin (Zhou et al., 2007; Lin et al., 2016), Felsic on western Yangtze side of Nanhua Basin (Wang, et al., 2012b).

Fig. 8(a-f). Relationship diagram between major elements and SiO_2 contents for felsic volcanic rocks of the Louqian Formation. Comparative data are fromLi et al., 2003;Li

et al., 2018b; Lin et al., 2016; Luo et al., 2018; Wang et al., 2008; Wang et al., 2010; Wang et al., 2012b; Yao et al., 2014a; Zheng et al., 2008; Zhou et al., 2007. (g) A/CNK (Al_2O_3/(CaO + Na_2O + K_2O))versus ANK (Al_2O_3 + Na_2O + K_2O) (Maniarand Piccoli, 1989). (h)Zr/TiO_2 versus Nb/Y diagram (Winchester and Floyd, 1977). Comparative data are fromLi et al., 2003;Li et al., 2018b; Lin et al., 2016; Luo et al., 2018; Wang et al., 2008; Wang et al., 2010; Wang et al., 2012b; Yao et al., 2014a; Zheng et al., 2008; Zhou et al., 2007.

Fig. 9. Chondrite normalized rare earth element (REE) patterns (a) and primitivemantle normalized multi-element profiles (b) of the Louqian Rhyolite tuff. Chondrite and primitive mantle normalizing values are from Boynton (1984) andSun and McDonough (1989), respectively. Comparative data are from Drummond et al., 2011; Li et al., 2003;Li et al., 2018b; Wang et al., 2010;Yao et al., 2014a; Zheng et al., 2008.

Fig. 10. Plots of (a) 10000×Ga/Al versusZr+Nb+Ce+Y (Eby, 1992), (b)10000×Ga/Al versus(K_2O+Na_2O)/CaO(Whalen et al., 1987), (c) Y/Nb versus Rb/Nb (Eby, 1992), and (d) Nb-Y-Ce (Eby, 1992). Comparative data are fromDrummond et al., 2011; Li et al., 2003;Li et al., 2018b; Wang et al., 2010;Yao et al., 2014a; Zheng et al., 2008. (e)Plots of (Na+K+2Ca)/(Al×Si) versus Zr (ppm) (Watson et al., 1983). Comparative data are from Drummond et al., 2011; Li et al., 2003;Li et al., 2018b; Wang et al.,

2010;Yao et al., 2014a; Zheng et al., 2008.

Fig. 11. Plots of (a) Ta/Yb versus Th/Yb (Gorton and Schandl, 2000), (b) Nb+Y versus Rb (ppm) (Pearce et al., 1984), (c) Y versus Nb (Pearce et al., 1984), and (d) Yb+Ta versus Rb (ppm) (Pearce et al., 1984). Comparative data are from Drummond et al., 2011; Li et al., 2003;Li et al., 2018b; Wang et al., 2010;Yao et al., 2014a; Zheng et al., 2008.

Fig. 12 (a) Rodinia assembly at ca. 900 Ma (adapted Cawood et al., 2018), (b) Proposed tectonic setting and paleogeographic links between Neoproterozoic Panxi-Hannan Belt in South China with time equivalent igneous activity in northwest India, Seychellesand Madagascar(adaptedWang et al., 2017), and (c) A tectonic model for 770 Ma continental rifting associated with back-arc extension.

Table 1. List of reliable ages and zircon εHf(t) values of ca. 805~750 Ma igneous rocks in South China

	Batholith or Pluton/Group or Formation	Rock type	Age (Ma)	Method	Zircon εHf(t)	Reference
Central South China						
1	Hongchicun Formation	Intermediate to felsic volcanic rocks	797 ± 11 Ma	SHRIMP U-Pb zircon		Li et al. (2003)
2	Daolinshan	Granite	790 ± 6 Ma	LA-ICP-MS zircon	7.0 ~ 14.4	Yao et al. (2014)
			775 ± 13, 780 ± 5 Ma	SHRIMP and LA-ICP-MS U-Pb zircon	6.7 ~17.4	Wang et al. (2010)
			794 ± 9 Ma	SHRIMP U-Pb zircon		Li et al. (2008)
3	Shangshu Formation	Rhyolite	792 ± 5 Ma	SHRIMP U-Pb zircon		Li et al. (2008)
		Dacite-rhyolite	779± 7 Ma	LA-ICP-MS zircon		Wang et al. (2015)
		Tuff	767± 7 Ma	SHRIMP U-Pb zircon		Gao et al. (2008)
4	Puling Formation	Rhyolite, Tuff, Basalt	751 ± 8 ~ 765 ± 7 Ma	LA-ICP-MS zircon		Wang et al. (2012)
5	Jingtan Formation	Tuff, Dacite	773 ± 7 Ma , 779 ± 7 Ma	LA-ICP-MS zircon	0.7 ~6.8	Zheng et al. (2008)
			784~788 Ma	SIMS U-Pb zircon	1.26 ~ 11.6	Li et al.(2018)
6	Shi'ershan	Leucogranite	779 ± 11 Ma	SHRIMP U-Pb zircon		Li et al. (2003)
		Shi'ershan Granitic porphyry	785 ± 11 Ma	LA-ICP-MS zircon		Xue et al. (2010)
		Lianhuashan Granite	771 ± 17 Ma	SHRIMP U-Pb zircon	4.4 ~ 8.4	Zheng et al. (2008)
			777 ± 7 Ma	LA-ICP-MS U-Pb zircon		

		Qixitian Granite	775 ± 5 Ma	LA-ICP-MS U-Pb zircon	0.9 ~8.5	
		Granite	779 ± 11 Ma	LA-ICP-MS U-Pb zircon	2.9 ~ 6.6	Wang et al. (2013)
7	Shangshu Formation	Dacite,Rhyolite	794 ± 7 ~ 797 ± 5 Ma	LA-ICP-MS zircon		Wang et al. (2012)
8	Qingshuijiang	Tuff	774 ± 5 Ma	SHRIMP U-Pb zircon		Wang et al. (2012)
			774 ± 8 Ma	SHRIMP U-Pb zircon		Gao et al. (2010)
			780 ± 9 Ma	SHRIMP U-Pb zircon		Wang et al. (2010)
9	Ejiaao	Tuff	783 ± 9 Ma	SHRIMP U-Pb zircon		Wang et al. (2010)
10	Sanmenjie	Dacite,Rhyolite	765 ± 14 Ma	SHRIMP U-Pb zircon		Zhou et al. (2007)
11	Tongdao	Pyroxenite	772 ± 11 Ma	SHRIMP U-Pb zircon	-0.86~3.93	Wang et al. (2008)
12	Longsheng	Gabbro	761 ± 8 Ma			Ge et al. (2001)
		Peridotite	770 Ma	LA-ICP-MS U-Pb zircon		Chen (2018)
		Peridotite	760 ± 18 Ma	Single-grain zircon TIMS		Lin et al. (2016)
Eastern South China						
13	Zhenghe	Diabase	795 ± 7 Ma	SHRIMP U-Pb zircon		Shu et al. (2008b)

Table 2. Major and trace element compositions of rhyolite tuffs from Louqian Formation on the eastern South China Craton.

Sample	PM01-1	PM01-2	PM01-3	PM01-4	PM01-5	PM01-6	PM01-7	PM01-9	PM01-10	PM01-11	PM01-12	PM01-13	PM01-14	PM01-15	PM01-16	PM01-17	PM01-18	PM01-19
SiO_2	72.11	68.62	72.3	69.21	71.22	69.65	65.11	74.26	71.96	66.41	68.78	68.83	68.78	79.81	71.12	68.13	61.58	57.8
TiO_2	0.25	0.34	0.32	0.3	0.34	0.38	0.45	0.33	0.25	0.49	0.34	0.71	1.14	0.28	0.32	0.55	1	0.81
Al_2O_3	14.65	15.87	13.64	15.64	14.04	15.88	17.32	14.09	14.35	15.3	18.39	14.38	13.3	9.79	14.8	15.52	16.2	16.55
TFe_2O_3	2.68	3.21	2.92	2.85	2.91	2.83	4.27	1.85	1.71	3.34	3.16	4.81	6.28	1.61	2.54	3.86	8.56	8.58
MnO	0.05	0.02	0.05	0.05	0.12	0.05	0.05	0.05	0.05	0.08	0.07	0.06	0.14	0.05	0.04	0.04	0.03	0.08
MgO	1.11	0.68	0.76	1.07	0.68	0.98	1.35	0.65	0.45	1.03	1.34	1.26	0.98	1.39	0.8	2.63	3.34	3.97
CaO	0.1	0.06	0.12	0.35	0.05	0.11	0.12	0.06	0.55	1.31	0.08	0.16	0.59	0.61	0.13	0.18	0.02	1.13
Na_2O	1.98	4.41	4.08	3.04	1.7	2.84	1.4	1.82	4.65	4.51	3.68	2.15	2.84	2.04	2.56	3.84	0.05	0.8
K_2O	4.23	4.21	3.69	5.17	6.26	5	6.9	4.65	3.92	4.13	5.54	3.61	3.45	2.15	4.85	2.63	4.02	4.72
P_2O_5	0.02	0.04	0.06	0.03	0.05	0.05	0.08	0.01	0.04	0.11	0.06	0.04	0.13	0.11	0.04	0.1	0.06	0.2
LOI	2.8	1.75	1.13	1.82	1.81	2.04	2.77	2.13	1.31	2.33	0.53	3.02	2.26	1.82	1.96	2.44	4.38	4.6
Total	100.06	99.34	99.27	99.66	99.55	99.97	100.01	100.08	99.37	99.17	102.18	99.18	100.05	99.73	99.33	100.02	99.36	99.36
CIA	57.89	45.47	44.26	53.26	59.42	52.27	59.07	56.72	46.46	55.55	50.38	58.17	55.78	61.15	52.83	50.53	78.47	71.17
Sc	5.9	8.5	6.1	7.2	8.2	7.4	8.7	6.5	5.1	8	6.7	10.9	11.6	6.6	6.5	9.3	20.4	18.3
V	12	23	27	11	18	27	35	22	19	41	20	88	103	26	28	79	132	107
Cr	20	10	20	10	20	20	30	10	20	10	<10	40	60	20	10	30	100	110
Co	5	4.6	4.6	2.8	2.9	4.4	6.2	2.2	2.1	4.2	4.9	9.1	11.6	3.9	3.8	6.4	31.4	26.7
Ga	20.3	17.1	16.5	24.2	20.9	19.9	23	19.9	17.7	17.6	27.5	18.8	18.4	13	17.2	19.1	24.5	25.1
Rb	180	141	114.5	221	240	177.5	297	167.5	99.8	143	175.5	130	119.5	73.8	187	88.2	167	191.5
Sr	66.6	90	92.3	90.4	99.1	52.1	69.2	64.8	104.5	127	37	54.5	87.1	43.5	73.4	82.5	11.8	36.1
Y	27.6	24	21.9	30.6	43.6	30.4	39	30.9	27.5	21.1	26.4	24.9	29.6	19.3	28.6	27.7	48.5	35.5

Zr	188	199	213	287	225	237	245	302	215	214	227	325	582	146	204	227	189	124
Nb	28.4	16.8	14.9	21	18.4	14.6	18.1	16.5	15.3	11.8	14.2	16.7	22.5	10.2	14.1	11.5	18.9	17.4
La	32.2	65.8	50	59	113	73.1	81.5	47.4	45	43.6	64.9	54.2	74.5	35.3	80.8	44.7	60.4	69
Ce	61.5	102.5	90.3	96.7	143.5	88.2	133	90.6	86.6	83.1	117	97.5	135	69.9	104	77.3	101	129.5
Pr	6.86	13.75	10.2	12.15	21.1	18.4	16.1	10.55	9.6	9.38	13.7	11.55	14.95	7.99	16.85	9.46	14.3	16.05
Nd	22.9	46.1	33.7	41.4	72.1	63.3	54.8	36.6	32.9	32.6	47.8	39.2	49.9	27.8	57	34.3	52.5	57.3
Sm	4.69	7.38	5.25	6.93	11.55	10.3	8.83	6.37	5.51	5.33	7.88	6.34	7.59	4.66	9.04	6	9.1	9.57
Eu	0.42	1.22	0.95	0.95	1.65	2	1.56	0.82	0.87	1.28	1.43	1.38	1.51	0.88	1.71	1.49	2.02	1.97
Gd	4.44	5.74	4.39	5.63	10.35	7.55	7.6	5.39	4.92	4.66	6.05	5.08	6.06	3.84	7.15	5.41	8.53	8.21
Tb	0.76	0.83	0.67	0.87	1.5	1.13	1.14	0.83	0.77	0.65	0.87	0.77	0.91	0.56	1.03	0.85	1.3	1.2
Dy	4.72	4.46	4.06	5.3	8.52	6.3	6.59	5.28	4.71	3.88	4.9	4.49	5.32	3.36	6.12	4.92	7.7	6.73
Ho	1.01	0.89	0.85	1.1	1.59	1.17	1.33	1.13	1.02	0.78	1	0.92	1.12	0.69	1.11	1.01	1.54	1.34
Er	3.14	2.53	2.45	3.32	4.02	3.27	3.82	3.33	2.84	2.18	2.99	2.63	3.19	2	3.01	2.92	4.26	3.51
Tm	0.54	0.4	0.38	0.56	0.63	0.47	0.57	0.54	0.46	0.33	0.45	0.41	0.52	0.32	0.46	0.44	0.64	0.51
Yb	3.64	2.62	2.54	3.79	3.76	2.99	3.53	3.53	2.96	2.26	2.81	2.76	3.37	2.09	2.88	2.7	3.98	3.13
Lu	0.61	0.42	0.4	0.62	0.56	0.49	0.55	0.56	0.49	0.36	0.46	0.45	0.55	0.35	0.44	0.43	0.62	0.47
Hf	7	6	6.1	8.6	6.4	6.8	7.1	8.6	6.5	6	7.1	9	15.1	4.4	5.9	6.4	5.7	3.7
Ta	2.3	1.3	1.2	1.5	1.4	1.1	1.3	1.1	1	0.7	1.1	1.1	1.4	0.7	1	0.8	1.2	1
Th	28.7	19.5	16.8	22.2	22.2	16.4	19.55	12.15	11.5	9.26	14.75	13.8	18.55	7.85	16.7	9.03	15.3	19.05
T^{Zr} (°C)	850	825	831	866	850	857	865	896	819	807	845	905	945	817	843	855	879	803

Major element contents in wt% and trace element concentrations in ppm.

Highlights

- Rhyolite tuffs with age of ca.770 Ma have been recognized in the Cathaysia Block.
- Rhyolite tuffs are A-type and display arc-affinity.
- The Nanhua basin was located in the back arc setting along the periphery of Rodinia.

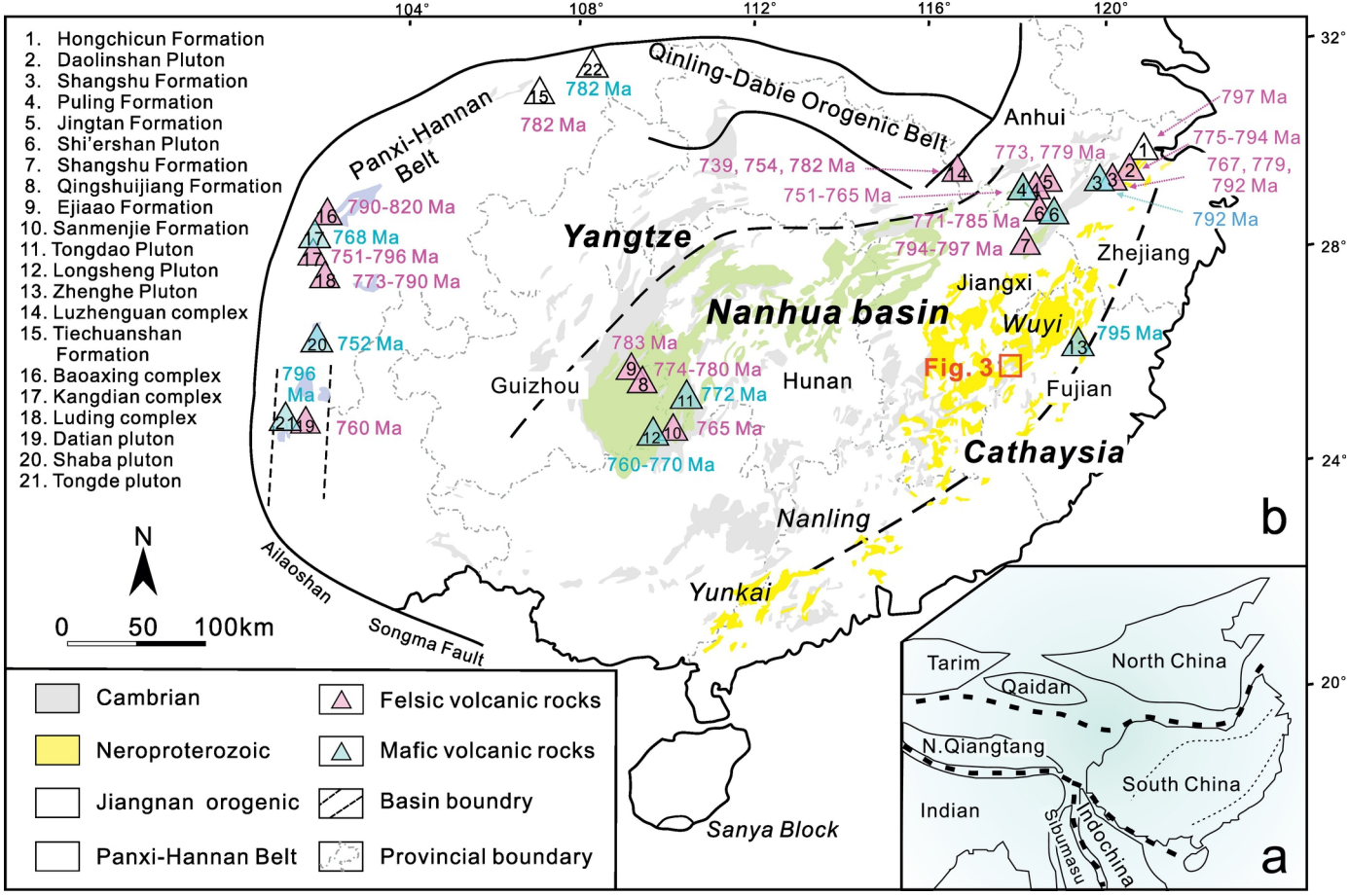
1. Hongchicun Formation
2. Daolinshan Pluton
3. Shangshu Formation
4. Puling Formation
5. Jingtan Formation
6. Shi'ershan Pluton
7. Shangshu Formation
8. Qingshuijiang Formation
9. Ejiaao Formation
10. Sanmenjie Formation
11. Tongdao Pluton
12. Longsheng Pluton
13. Zhenghe Pluton
14. Luzhenguan complex
15. Tiechuanshan Formation
16. Baoaxing complex
17. Kangdian complex
18. Luding complex
19. Datian pluton
20. Shaba pluton
21. Tongde pluton
104°
108°
112°
116°
120°
32°
28°
24°
20°
Panxi-Hannan Belt
Qinling-Dabie Orogenic Belt
Yangtze
Nanhua basin
Cathaysia
Nanling
Yunkai
Anhui
Zhejiang
Jiangxi
Fujian
Hunan
Guizhou
Wuyi
Fig. 3
782 Ma
782 Ma
790-820 Ma
768 Ma
751-796 Ma
773-790 Ma
752 Ma
796 Ma
760 Ma
783 Ma
774-780 Ma
772 Ma
765 Ma
760-770 Ma
739, 754, 782 Ma
751-765 Ma
771-785 Ma
794-797 Ma
773, 779 Ma
797 Ma
775-794 Ma
767, 779, 792 Ma
792 Ma
795 Ma
Ailaoshan
Songma Fault
Sanya Block
N
0 50 100km
Cambrian
Neroproterozoic
Jiangnan orogenic
Panxi-Hannan Belt
Felsic volcanic rocks
Mafic volcanic rocks
Basin boundry
Provincial boundary
Tarim
North China
Qaidan
N.Qiangtang
South China
Indian
Sibumasu
Indochina
a
b

Figure 1

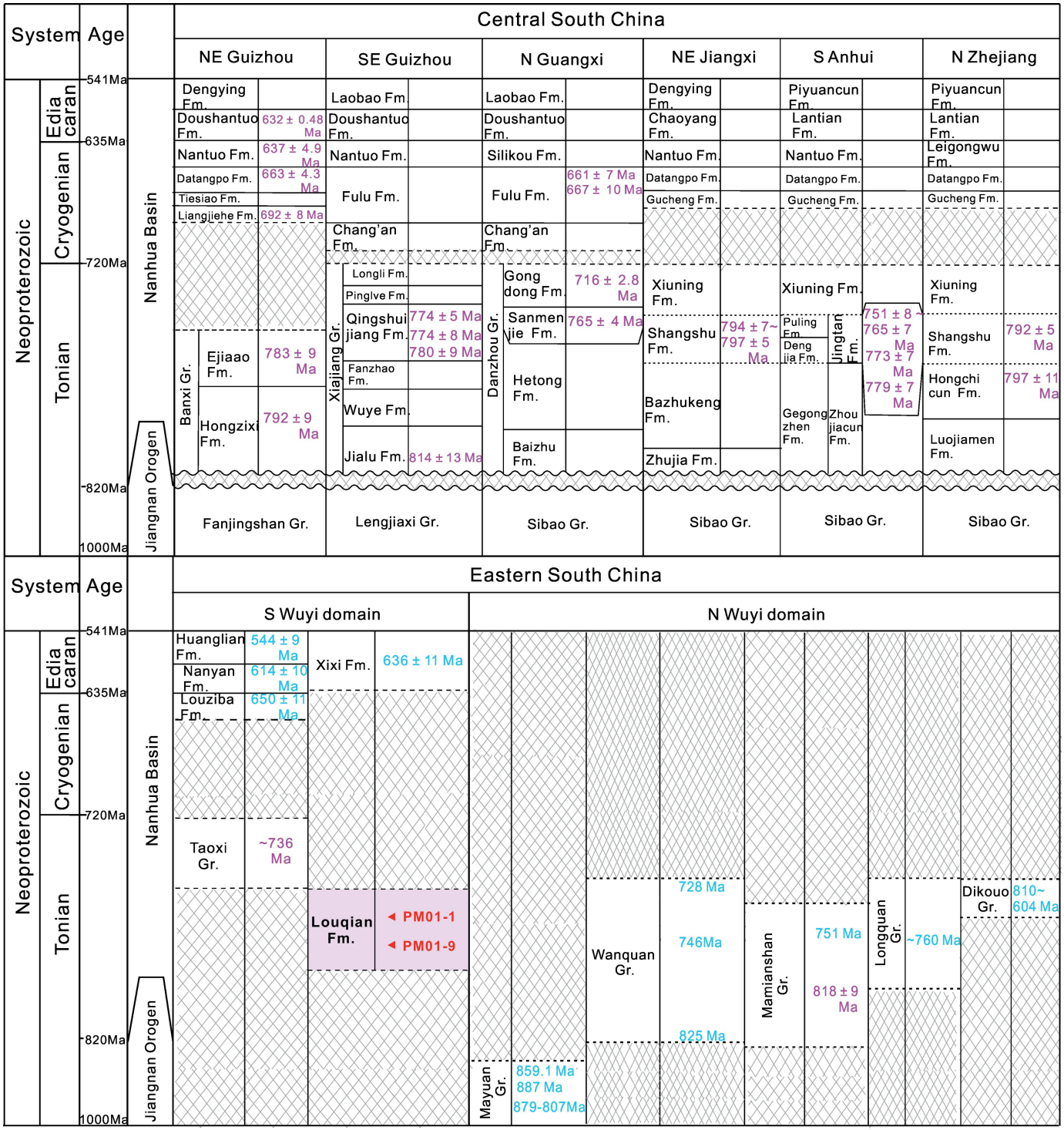
Central South China
System
Age
NE Guizhou
SE Guizhou
N Guangxi
NE Jiangxi
S Anhui
N Zhejiang
Neoproterozoic
Ediacaran
Cryogenian
Tonian
541Ma
635Ma
720Ma
820Ma
1000Ma
Nanhua Basin
Jiangnan Orogen
Dengying Fm.
Doushantuo Fm.
632 ± 0.48 Ma
Nantuo Fm.
637 ± 4.9 Ma
Datangpo Fm.
663 ± 4.3 Ma
Tiesiao Fm.
Liangjiehe Fm.
692 ± 8 Ma
Banxi Gr.
Ejiaao Fm.
783 ± 9 Ma
Hongzixi Fm.
792 ± 9 Ma
Fanjingshan Gr.
Laobao Fm.
Doushantuo Fm.
Fulu Fm.
Chang'an Fm.
Xiajiang Gr.
Longli Fm.
Pinglve Fm.
Qingshuijiang Fm.
774 ± 5 Ma
774 ± 8 Ma
780 ± 9 Ma
Fanzhao Fm.
Wuye Fm.
Jialu Fm.
814 ± 13 Ma
Lengjiaxi Gr.
Laobao Fm.
Doushantuo Fm.
Silikou Fm.
Fulu Fm.
661 ± 7 Ma
667 ± 10 Ma
Chang'an Fm.
Danzhou Gr.
Gongdong Fm.
716 ± 2.8 Ma
Sanmenjie Fm.
765 ± 4 Ma
Hetong Fm.
Baizhu Fm.
Sibao Gr.
Dengying Fm.
Chaoyang Fm.
Nantuo Fm.
Datangpo Fm.
Gucheng Fm.
Xiuning Fm.
Shangshu Fm.
794 ± 7~
797 ± 5 Ma
Bazhukeng Fm.
Zhujia Fm.
Sibao Gr.
Piyuancun Fm.
Lantian Fm.
Nantuo Fm.
Datangpo Fm.
Gucheng Fm.
Xiuning Fm.
Puling Fm.
Dengjia Fm.
Jingtan Fm.
751 ± 8 ~
765 ± 7 Ma
773 ± 7 Ma
779 ± 7 Ma
Gegongzhen Fm.
Zhoujiacun Fm.
Sibao Gr.
Piyuancun Fm.
Lantian Fm.
Leigongwu Fm.
Datangpo Fm.
Gucheng Fm.
Xiuning Fm.
Shangshu Fm.
792 ± 5 Ma
Hongchicun Fm.
797 ± 11 Ma
Luojiamen Fm.
Sibao Gr.
Eastern South China
S Wuyi domain
N Wuyi domain
Huanglian Fm.
544 ± 9 Ma
Nanyan Fm.
614 ± 10 Ma
Louziba Fm.
650 ± 11 Ma
Xixi Fm.
636 ± 11 Ma
Taoxi Gr.
~736 Ma
Louqian Fm.
PM01-1
PM01-9
Mayuan Gr.
859.1 Ma
887 Ma
879-807Ma
Wanquan Gr.
728 Ma
746Ma
825 Ma
Mamianshan Gr.
751 Ma
818 ± 9 Ma
Longquan Gr.
~760 Ma
Dikouo Gr.
810~
604 Ma
Disconformity
Augular unconformity
Stratigraphic hiatus
Sample location
783 ± 9 Ma
Dating results from igenous, tuff or metavolcanic rocks
544 ± 7 Ma
Dating results from siliciclastic or zircon core ages from metamorphic rocks

Figure 2

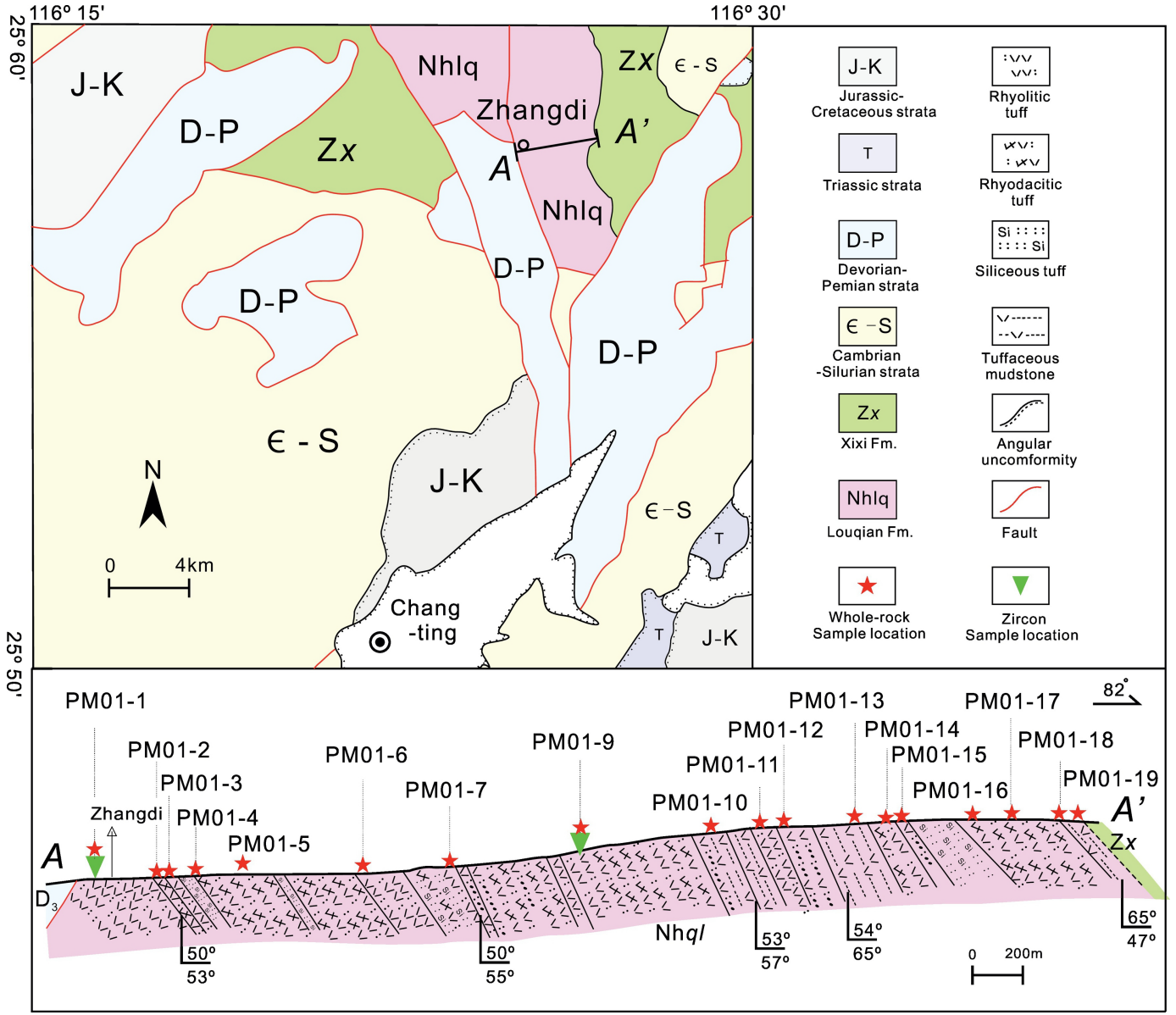
116° 15'
116° 30'
25° 60'
25° 50'
J-K
D-P
Zx
Nhlq
Zhangdi
A
A'
∈ - S
T
N
0
4km
Chang
-ting
Jurassic-
Cretaceous strata
Triassic strata
Devorian-
Pemian strata
Cambrian
-Silurian strata
Xixi Fm.
Louqian Fm.
Whole-rock
Sample location
Rhyolitic
tuff
Rhyodacitic
tuff
Siliceous tuff
Tuffaceous
mudstone
Angular
uncomformity
Fault
Zircon
Sample location
PM01-1
PM01-2
PM01-3
PM01-4
PM01-5
PM01-6
PM01-7
PM01-9
PM01-10
PM01-11
PM01-12
PM01-13
PM01-14
PM01-15
PM01-16
PM01-17
PM01-18
PM01-19
82°
D3
Nhql
50°
53°
50°
55°
53°
57°
54°
65°
65°
47°
0
200m

Figure 3


Centimeter
(a)
PM01-1
rhyotaxitic fluidal structure
500 μm
(b)
(c)
PM01-9
Q
Chl
Pl
Bt
200 μm
(d)
Centimeter
(e)
PM01-16
Pl
plastic vitric fragment
500 μm
(f)
Centimeter
(g)
PM01-19
500 μm
(h)

Figure 4

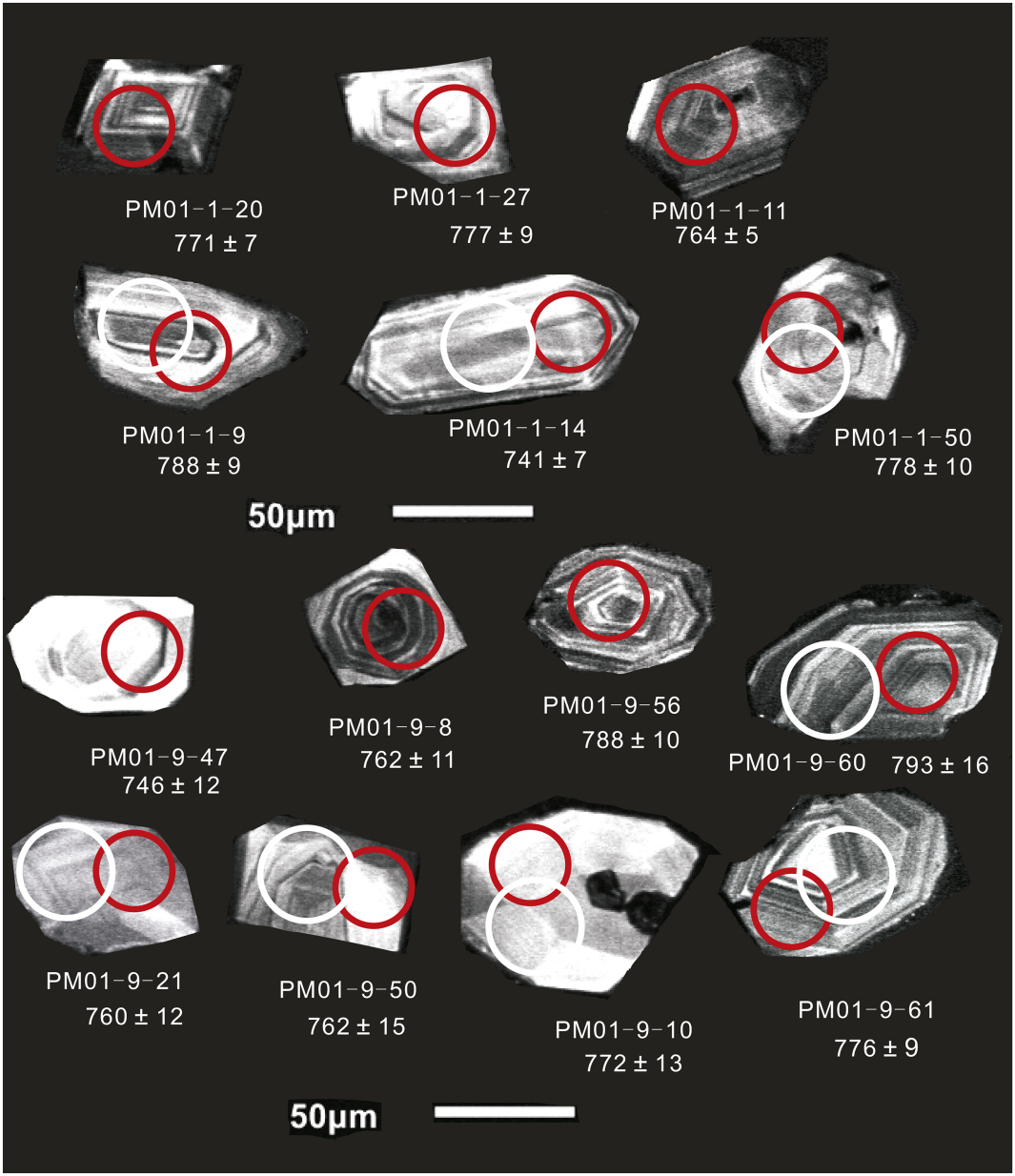
PM01-1-20
771 ± 7
PM01-1-27
777 ± 9
PM01-1-11
764 ± 5
PM01-1-9
788 ± 9
PM01-1-14
741 ± 7
PM01-1-50
778 ± 10
50μm
PM01-9-47
746 ± 12
PM01-9-8
762 ± 11
PM01-9-56
788 ± 10
PM01-9-60
793 ± 16
PM01-9-21
760 ± 12
PM01-9-50
762 ± 15
PM01-9-10
772 ± 13
PM01-9-61
776 ± 9
50μm

Figure 5

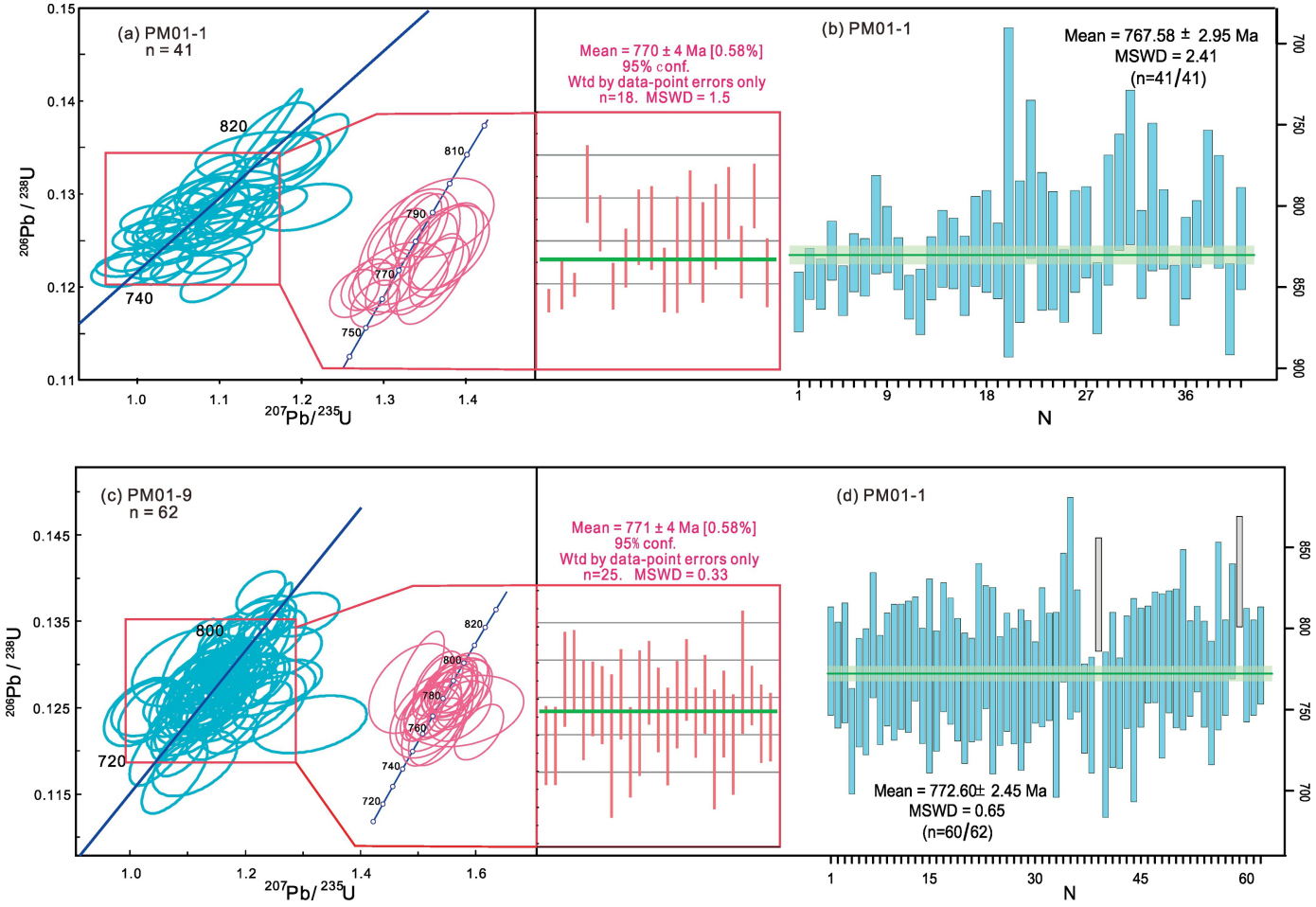
(a) PM01-1
n = 41
820
810
790
770
750
740
Mean = 770 ± 4 Ma [0.58%]
95% conf.
Wtd by data-point errors only
n=18. MSWD = 1.5
(b) PM01-1
Mean = 767.58 ± 2.95 Ma
MSWD = 2.41
(n=41/41)
206Pb / 238U
207Pb/235U
N
(c) PM01-9
n = 62
800
820
780
760
740
720
Mean = 771 ± 4 Ma [0.58%]
95% conf.
Wtd by data-point errors only
n=25. MSWD = 0.33
(d) PM01-1
Mean = 772.60± 2.45 Ma
MSWD = 0.65
(n=60/62)

Figure 6

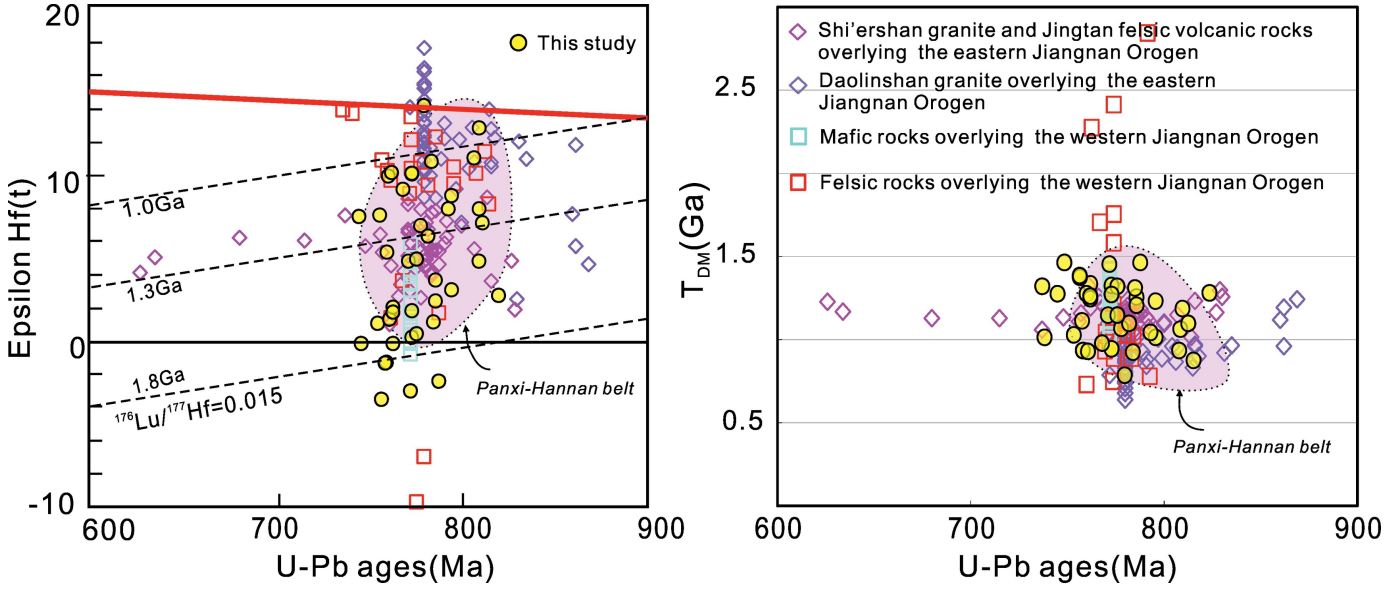
This study
1.0Ga
1.3Ga
1.8Ga
176Lu/177Hf=0.015
Panxi-Hannan belt
Epsilon Hf(t)
U-Pb ages(Ma)
Shi'ershan granite and Jingtan felsic volcanic rocks overlying the eastern Jiangnan Orogen
Daolinshan granite overlying the eastern Jiangnan Orogen
Mafic rocks overlying the western Jiangnan Orogen
Felsic rocks overlying the western Jiangnan Orogen
Panxi-Hannan belt
T DM(Ga)
U-Pb ages(Ma)

Figure 7

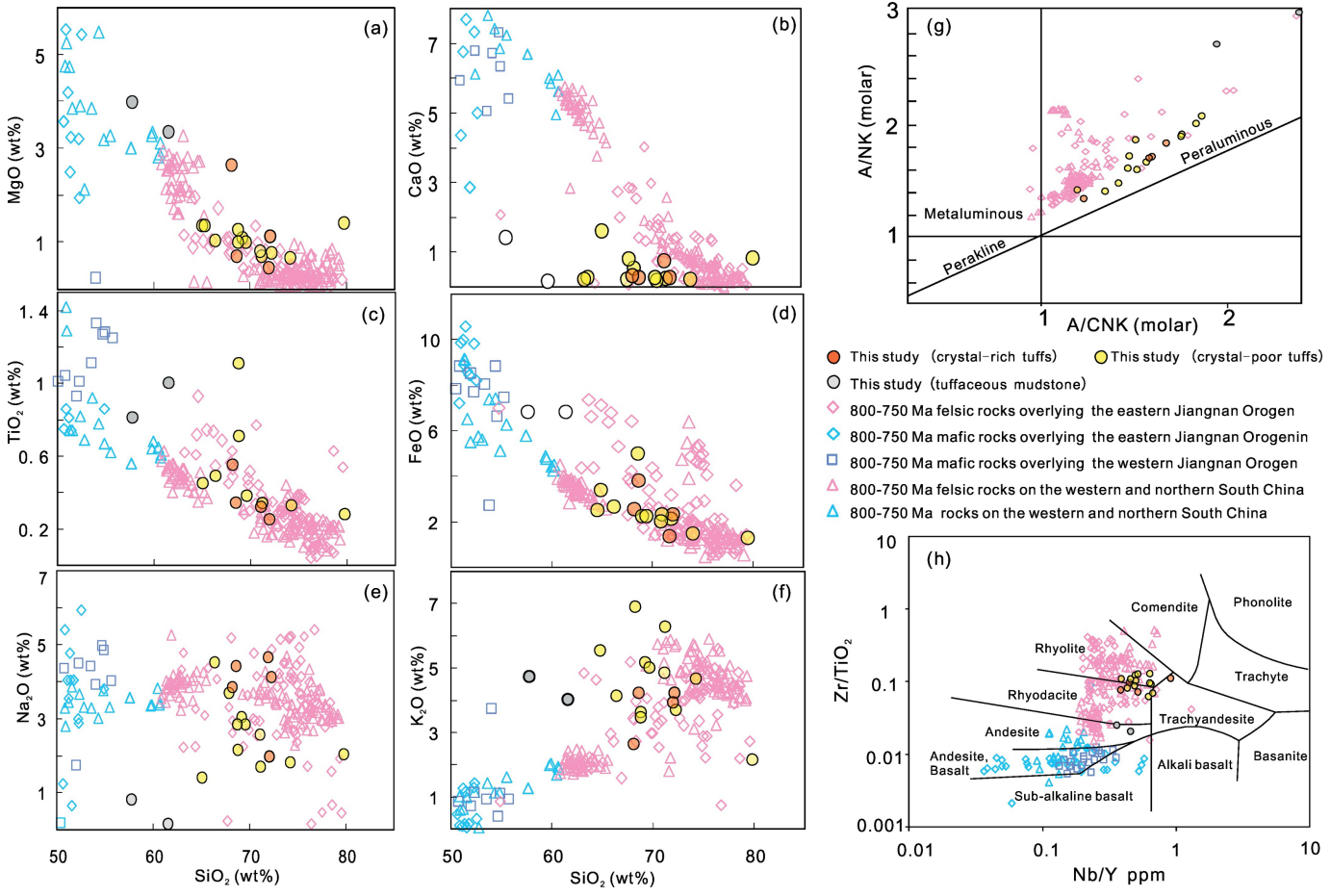
(a)
MgO (wt%)
(b)
CaO (wt%)
(c)
TiO2 (wt%)
(d)
FeO (wt%)
(e)
Na2O (wt%)
(f)
K2O (wt%)
SiO2 (wt%)
SiO2 (wt%)
(g)
A/NK (molar)
A/CNK (molar)
Peraluminous
Metaluminous
Perakline
This study (crystal-rich tuffs)
This study (crystal-poor tuffs)
This study (tuffaceous mudstone)
800-750 Ma felsic rocks overlying the eastern Jiangnan Orogen
800-750 Ma mafic rocks overlying the eastern Jiangnan Orogenin
800-750 Ma mafic rocks overlying the western Jiangnan Orogen
800-750 Ma felsic rocks on the western and northern South China
800-750 Ma rocks on the western and northern South China
(h)
Zr/TiO2
Nb/Y ppm
Comendite
Phonolite
Rhyolite
Trachyte
Rhyodacite
Trachyandesite
Andesite
Andesite, Basalt
Alkali basalt
Basanite
Sub-alkaline basalt

Figure 8

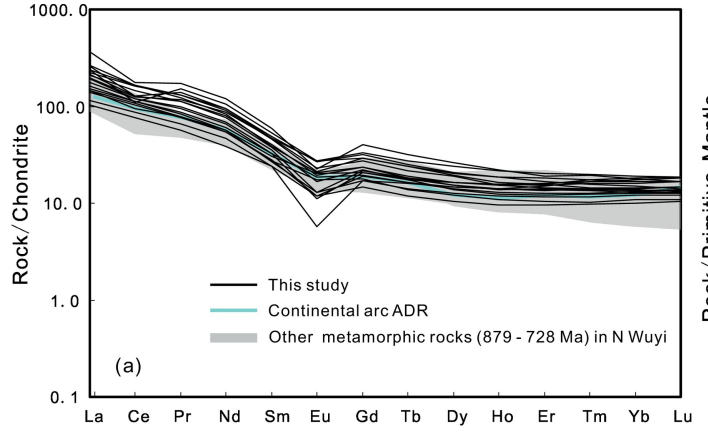
1000. 0
100. 0
10. 0
1. 0
0. 1
Rock/Chondrite
This study
Continental arc ADR
Other metamorphic rocks (879 - 728 Ma) in N Wuyi
(a)
La Ce Pr Nd Sm Eu Gd Tb Dy Ho Er Tm Yb Lu

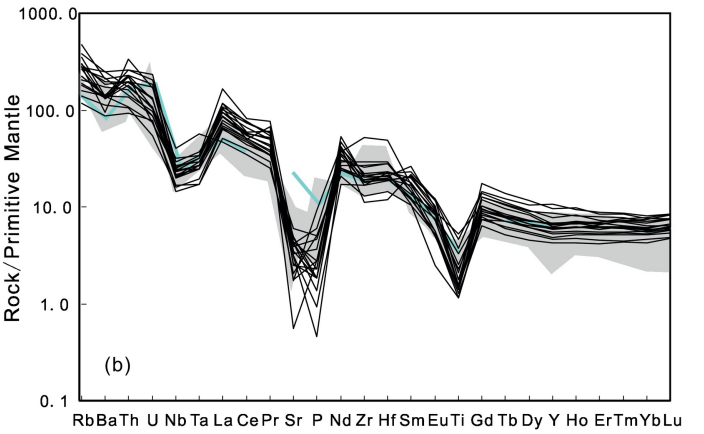
1000. 0
100. 0
10. 0
1. 0
0. 1
Rock/Primitive Mantle
(b)
Rb Ba Th U Nb Ta La Ce Pr Sr P Nd Zr Hf Sm Eu Ti Gd Tb Dy Y Ho Er Tm Yb Lu

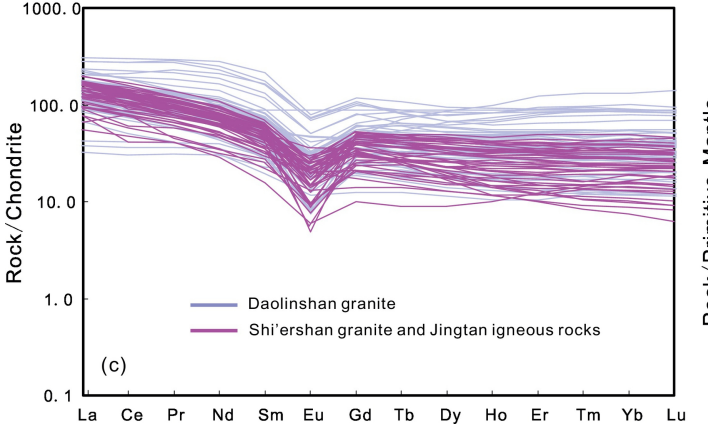
1000. 0
100. 0
10. 0
1. 0
0. 1
Rock/Chondrite
Daolinshan granite
Shi'ershan granite and Jingtan igneous rocks
(c)
La Ce Pr Nd Sm Eu Gd Tb Dy Ho Er Tm Yb Lu

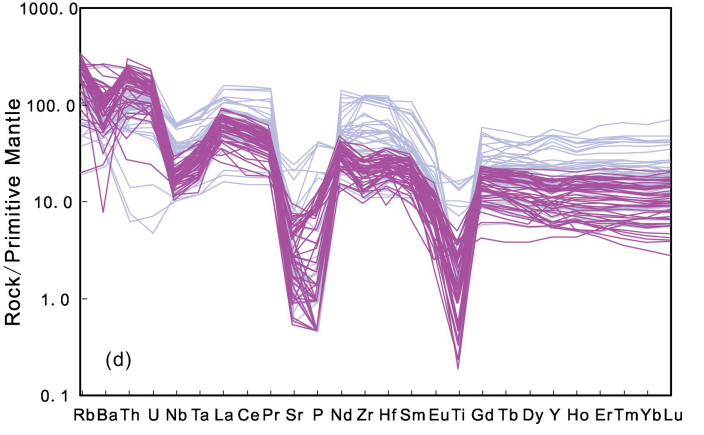
1000. 0
100. 0
10. 0
1. 0
0. 1
Rock/Primitive Mantle
(d)
Rb Ba Th U Nb Ta La Ce Pr Sr P Nd Zr Hf Sm Eu Ti Gd Tb Dy Y Ho Er Tm Yb Lu

Figure 9

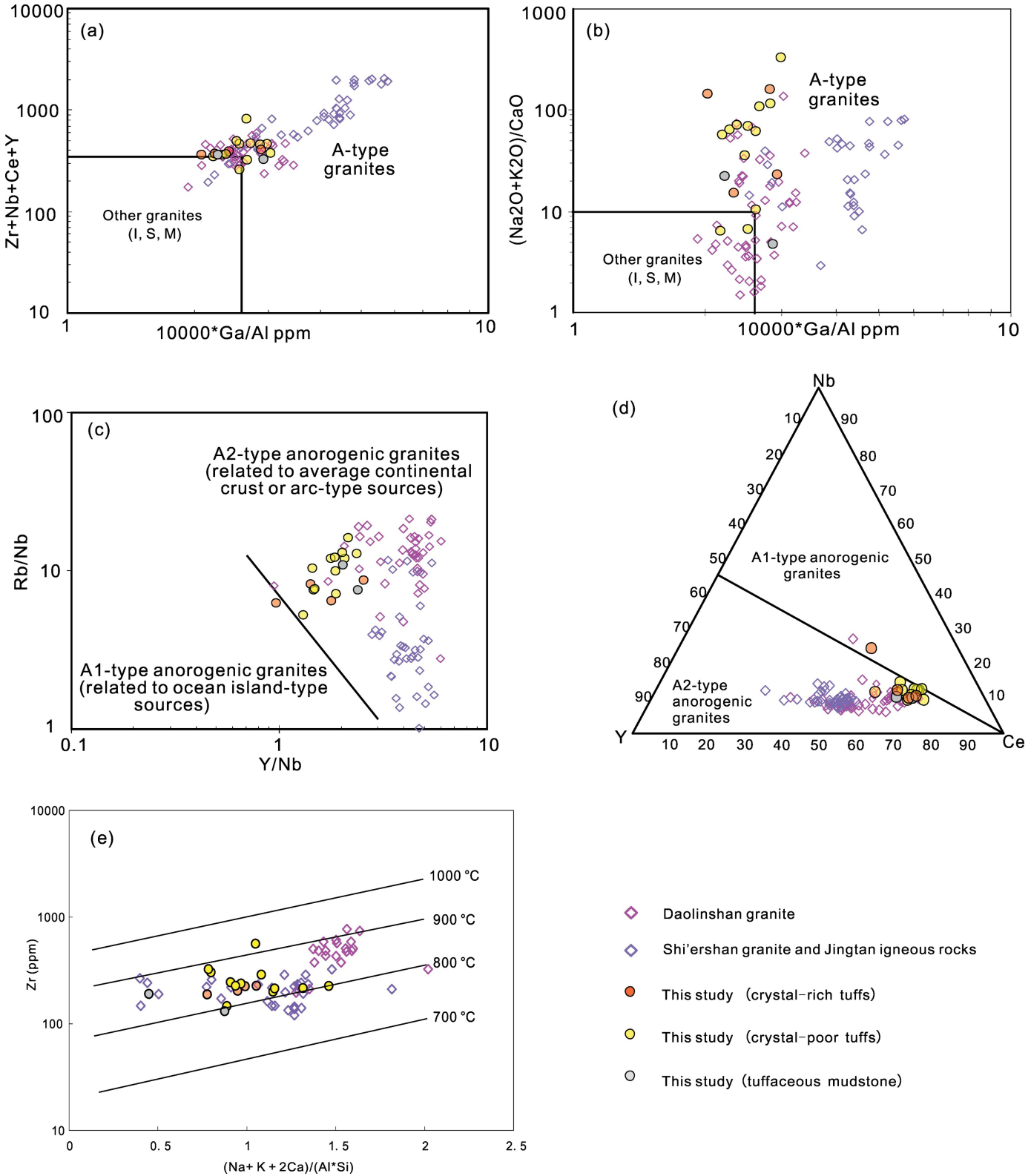
(a)
Zr+Nb+Ce+Y
10000*Ga/Al ppm
A-type granites
Other granites (I, S, M)
(b)
(Na2O+K2O)/CaO
10000*Ga/Al ppm
A-type granites
Other granites (I, S, M)
(c)
Rb/Nb
Y/Nb
A2-type anorogenic granites (related to average continental crust or arc-type sources)
A1-type anorogenic granites (related to ocean island-type sources)
(d)
Nb
Y
Ce
A1-type anorogenic granites
A2-type anorogenic granites
(e)
Zr (ppm)
(Na+ K + 2Ca)/(Al*Si)
1000 °C
900 °C
800 °C
700 °C
Daolinshan granite
Shi'ershan granite and Jingtan igneous rocks
This study (crystal-rich tuffs)
This study (crystal-poor tuffs)
This study (tuffaceous mudstone)

Figure 10

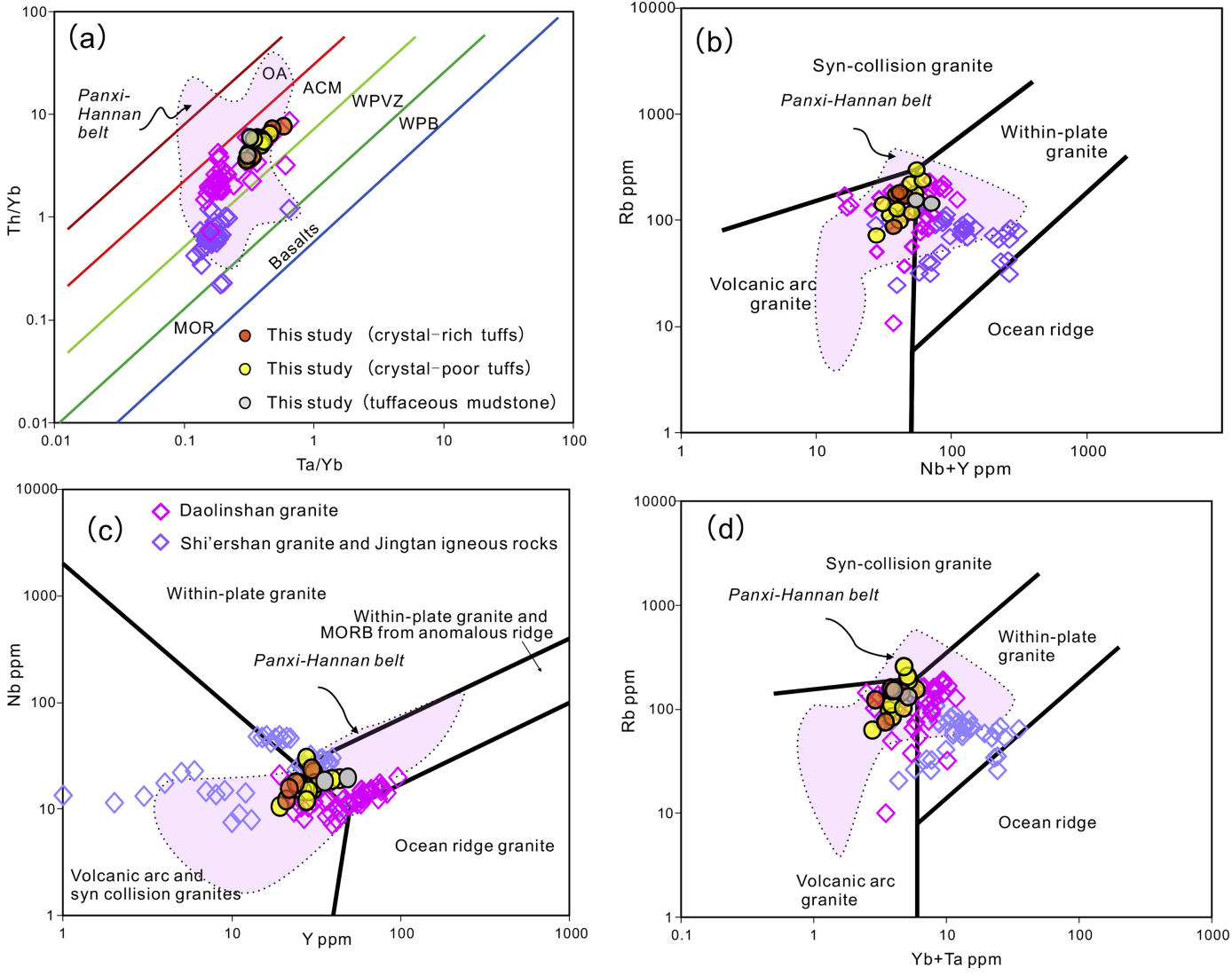
(a)
Panxi-Hannan belt
OA
ACM
WPVZ
WPB
Basalts
MOR
This study (crystal-rich tuffs)
This study (crystal-poor tuffs)
This study (tuffaceous mudstone)
Th/Yb
Ta/Yb
(b)
Syn-collision granite
Panxi-Hannan belt
Within-plate granite
Volcanic arc granite
Ocean ridge
Rb ppm
Nb+Y ppm
(c)
Daolinshan granite
Shi'ershan granite and Jingtan igneous rocks
Within-plate granite
Within-plate granite and MORB from anomalous ridge
Panxi-Hannan belt
Ocean ridge granite
Volcanic arc and syn collision granites
Nb ppm
Y ppm
(d)
Syn-collision granite
Panxi-Hannan belt
Within-plate granite
Ocean ridge
Volcanic arc granite
Rb ppm
Yb+Ta ppm

Figure 11

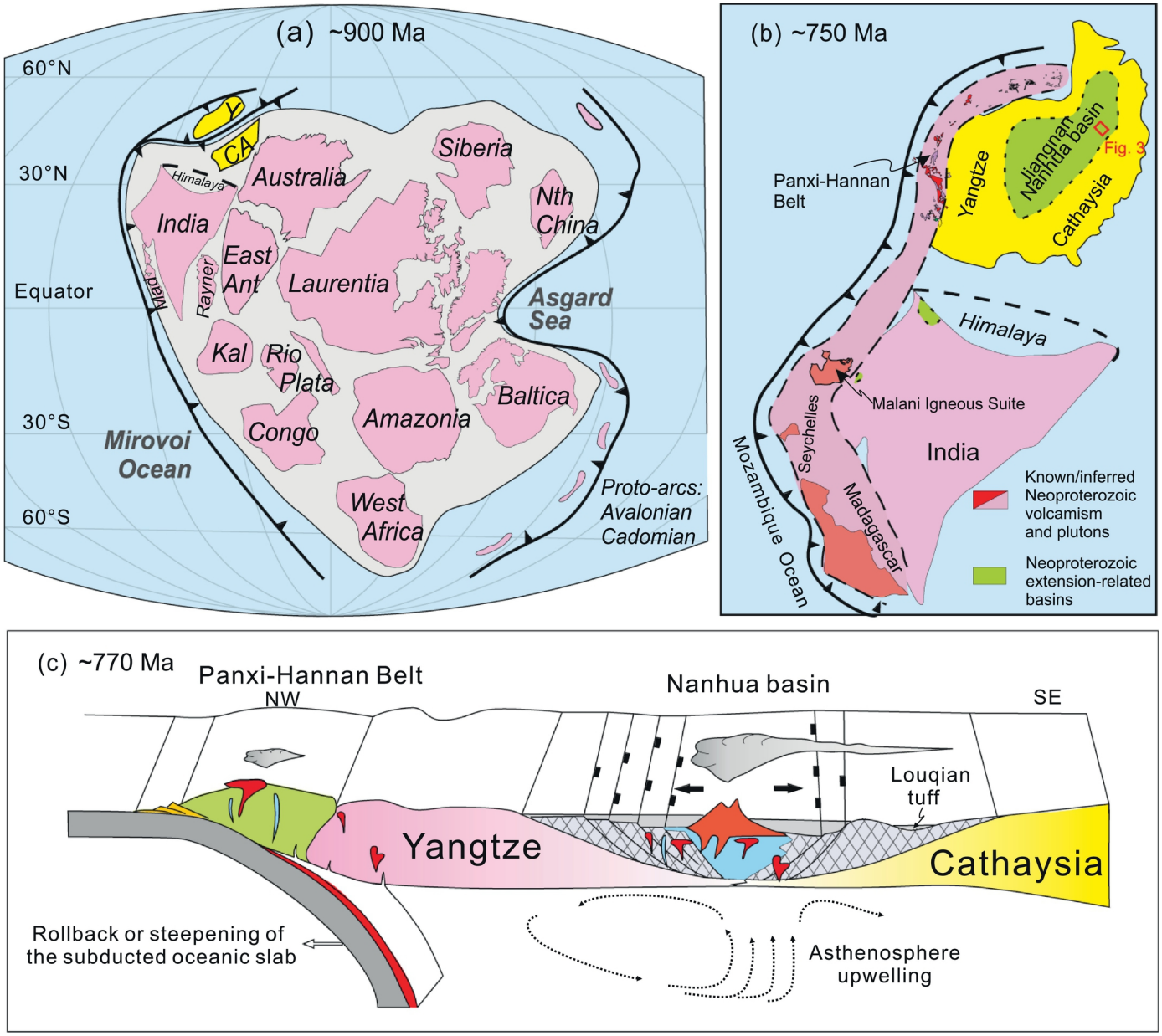
(a) ~900 Ma
60°N
30°N
Equator
30°S
60°S
Y
CA
Himalaya
India
Australia
Siberia
Nth China
East Ant
Laurentia
Mawson
Rayner
Asgard Sea
Kal
Rio Plata
Baltica
Amazonia
Congo
Mirovoi Ocean
West Africa
Proto-arcs:
Avalonian
Cadomian
(b) ~750 Ma
Panxi-Hannan Belt
Yangtze
Jiangnan
Nanhua basin
Fig. 3
Cathaysia
Himalaya
Malani Igneous Suite
Seychelles
India
Madagascar
Mozambique Ocean
Known/inferred Neoproterozoic volcamism and plutons
Neoproterozoic extension-related basins
(c) ~770 Ma
Panxi-Hannan Belt
NW
Nanhua basin
SE
Louqian tuff
Yangtze
Cathaysia
Rollback or steepening of the subducted oceanic slab
Asthenosphere upwelling

Figure 12